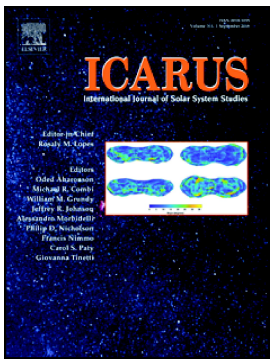

Pluto's far side

S.A. Stern, O.L. White, P.J. McGovern, J.T. Keane, J.W. Conrad, C.J. Bierson, T.R. Lauer, C.B. Olkin, L.A. Young, P.M. Schenk, J.M. Moore, H.A. Weaver, K.D. Runyon, K. Ennico, The New Horizons Team

PII: S0019-1035(20)30189-5

DOI: https://doi.org/10.1016/j.icarus.2020.113805

Reference: YICAR 113805

To appear in: *Icarus*

Received date: 16 October 2019

Revised date: 27 March 2020

Accepted date: 31 March 2020

Please cite this article as: S.A. Stern, O.L. White, P.J. McGovern, et al., Pluto's far side, *Icarus* (2020), https://doi.org/10.1016/j.icarus.2020.113805

Pluto's Far Side

S.A. Stern
Southwest Research Institute

O.L. White
SETI Institute

P.J. McGovern
Lunar and Planetary Institute

J.T. Keane
California Institute of Technology and
Jet Propulsion Laboratory

J.W. Conrad, C.J. Bierson
University of California, Santa Cruz

T. R. Lauer
NSF's National Optical Infrared Astronomy Research Laboratory

C.B. Olkin and L.A. Young
Southwest Research Institute

P.M. Schenk
Lunar and Planetary Institute

J.M. Moore
NASA Ames Research Center

H.A. Weaver and K.D. Runyon
Johns Hopkins University, Applied Physics Laboratory

K. Ennico
NASA Ames Research Center

and The New Horizons Team

Abstract

The New Horizons spacecraft provided near-global observations of Pluto that far exceed the resolution of Earth-based datasets. However, most previous Pluto New Horizons analyses focused on the New Horizons encounter hemisphere (i.e., the anti-Charon hemisphere containing Sputnik Planitia). In this work, we summarize and interpret data on Pluto's "far side" (i.e., its non-encounter or alternatively, its sub-Charon hemisphere), providing the first integrated New Horizons overview of Pluto's far side terrains. We find strong evidence for widespread bladed (i.e., aligned CH_4-mountain) deposits, evidence for an impact crater about as large as any on the "near side" hemisphere, evidence for complex lineations approximately antipodal to Sputnik Planitia that may be causally related, evidence that the far side maculae (i.e., equatorial dark regions) are smaller and more structured than Pluto's encounter hemisphere maculae, and more.

1. Introduction

Before the 2015 exploration of Pluto by New Horizons none of Pluto's surface features were known except by crude (though heroically derived) albedo maps, with resolutions of 300-500 km obtained using the Hubble Space Telescope (e.g., Buie et al. 1992, 1997, 2010) and Pluto-Charon mutual event techniques (e.g., Young & Binzel 1993, Young et al. 1999 2001). The flyby of Pluto by New Horizons revolutionized knowledge of Pluto in many ways (e.g., Stern et al. 2015, 2018 and references therein), including via the moderate and high-resolution imaging of its near side (i.e., closest approach) hemisphere.

However, owing to the fact that Pluto is a slow rotator with a 6.3872-day period, a single spacecraft fast flyby like New Horizons could only observe one hemisphere of the planet closely. Nonetheless, the flyby was planned to obtain daily or more frequent panchromatic and color images from the spacecraft's LORRI (LOng Range Reconnaissance Imager; Cheng et al. 2008) and MVIC (Multispectral Visible Imaging Cameras) medium focal length (Reuter et al. 2008) imagers for many days on approach as the planet rotated. The resolution of these images are factors of ~20-50× poorer than the global mosaics of the near side (henceforth, NS, which is also the anti-Charon hemisphere and the close approach hemisphere) (see Figure 1). However, these datasets still represent vast (i.e., 15-30×) resolution improvements over what was available prior to the New Horizons flyby on the Pluto far side terrains (henceforth, FS; which is also the sub-Charon hemisphere).

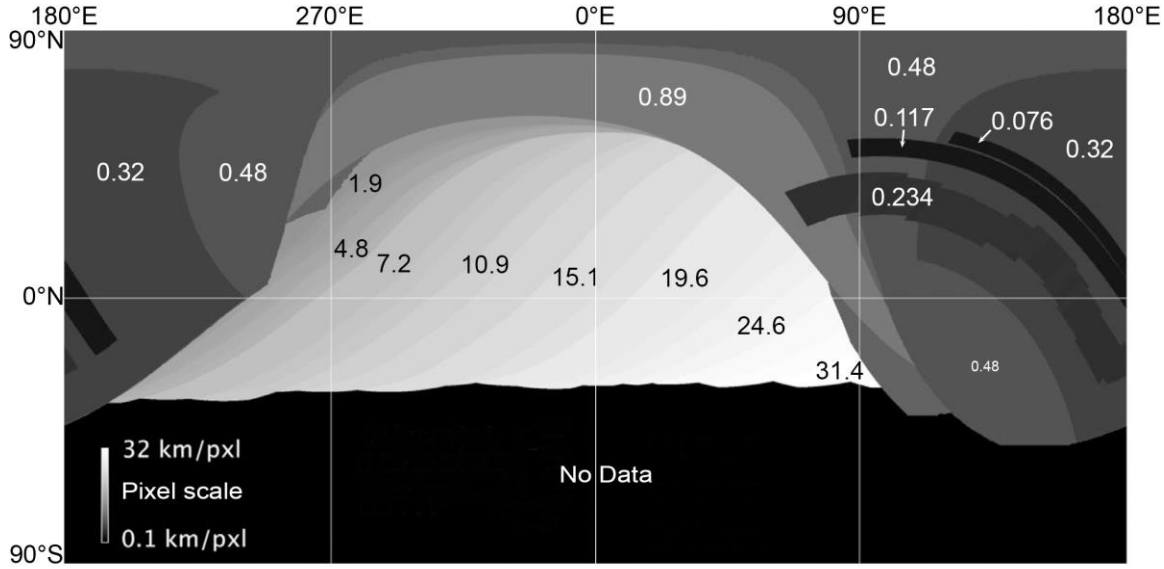

Figure 1. Global cylindrical map, centered on the FS at 0°E, illustrating the variation in pixel scale of the best New Horizons panchromatic imaging across Pluto. Note that the black region in the southern hemisphere was not imaged by New Horizons, as it was in winter darkness during the flyby.

In what follows here we summarize the main FS results obtained with the imagers aboard New Horizons and describe albedo, color, and geological interpretations of these data. We also point to specific needs for future work to learn even more about Pluto's FS, and to the prospects for future FS studies in the coming decades.

2. Far Side Maps

Here we present far side panchromatic and color mosaic products that feed our discussion of Pluto's FS. Figure 2 contains a global panchromatic map, which has a characteristic FS resolution of 20 km/pixel. Areas within the near side directly to the north, east, and west of the FS were observed at ~0.3-1 km/pixel resolutions, but areas within the FS were only imaged during the approach phase at pixel scales of 2 to 41 km/pixel.

In much of what follows, special processing was performed to maximize recovery of high-resolution information from the far-side LORRI images. In these cases, multiple images obtained at each epoch of observation

allowed for sub-sampled stacks to be constructed, from which the PSF was deconvolved; see Weaver et al. (2016) for further discussion of these image processing techniques.

For the purpose of geologically mapping the FS, this map has been modified from the official global map product described in Schenk et al. (2018) and archived in the PDS. Although positionally identical to those published maps, the high resolution mapping coverage within the FS shown in Figure 2 has been extended laterally by allowing larger emission angle data, and thus larger areas of the original images. The lower emission angle value cut-off was used in the earlier published product to reduce distortion in the map-projection, but was relaxed here in order to extend the highest resolution mapping into the FS as much as practical. In contrast, the low resolution imaging portion of the map was reprocessed with data observed at incidence and emission angles >72° and >50° omitted, respectively; this means slightly lower resolution data were mapped at each location, which removes oblique projection distortions inherent in the originally published map (which allowed incidence and emissions angles up to 82° and 78° respectively in this area, Schenk et al. 2018). This new, lower phase product emphasizes contrasts in surface albedo rather than shading due to topography, which is more conducive to contact definition and unit characterization when mapping the geology at pixel scales of kilometers to tens of kilometers per pixel.

For reference to other products used in the interpretations that follow, we also refer the reader to global color and composition maps that include FS terrains in Olkin et al. (2017) and Gabasova et al. (2020).

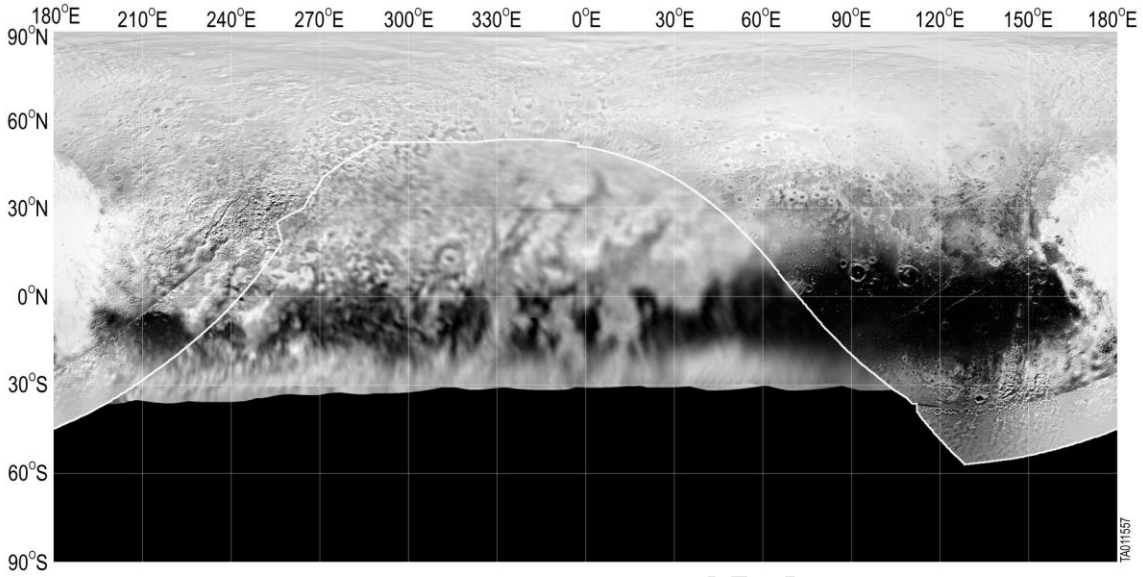

Figure 2. Global, panchromatic image mosaic of Pluto produced at 300 m/pixel. This cylindrical map projection is centered at 0°E on the far side; black areas below ~38°S were not illuminated during the New Horizons flyby. The area above the white arcuate line here NS hemisphere imaging (resolution better than 1 km/pixel); the area below the white line is covered only by far side imaging (>1 km/pixel resolution).

Figure 3, adapted from Buratti et al. (2017), shows a global bond albedo map. Inspecting Figures 2 and 3 reveals that the FS is more uniformly structured in latitude (i.e., zonally structured) than the NS, primarily due to the FS absence of the NS hemisphere's dominating albedo anomaly, Tombaugh Regio. It is also clear that the FS maculae (i.e., dark equatorial regions; see Stern et al. (2018)) are individually smaller (i.e., less extensive) and have more internal albedo variation than the maculae of the NS hemisphere; we discuss this in more detail later.

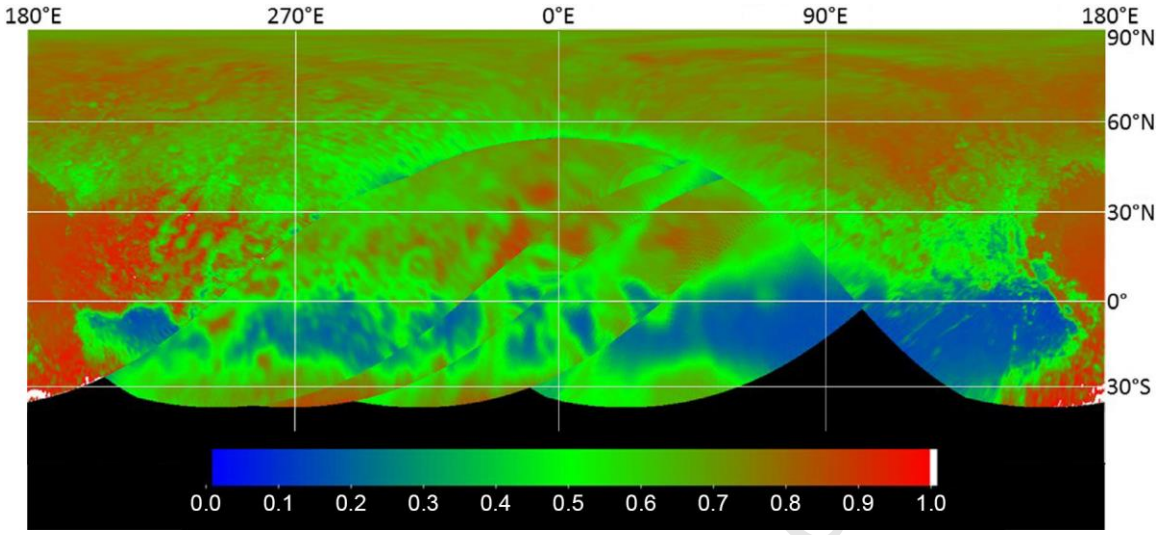

Figure 3. Pluto global Bond albedo map centered on Pluto's far side (adapted from Buratti et al 2017).

Figure 4a presents a global color map adapted from Schenk et al. (2018), using red, green and CH_4 MVIC color filter imaging. This map has been processed to maximize color differences and show the relative redness and blueness (i.e., spectral slope) of each color unit. Conclusions similar to those drawn from Figures 1 and 2 can be deduced here as well. Going further, as described in Schenk et al. (2018) and Moore et al. (2018), relatively bluish units are concentrated along the equatorial band between 30°N and 30°S.

Figure 4b presents a global map of CH_4 absorption derived from MVIC 890 nm filter imaging data; notice that the bluish units in Figure 4a stand out as areas of high CH_4 absorption in Figure 4b. These units have been ascribed by previously as related to the presence of 'bladed terrains' of aligned CH_4 mountains (Schenk et al. (2018) and Moore et al. (2018)), though there is somewhat more complex variegation in the distribution of the blue color units in Figure 4a. We discuss this further in the context of FS bladed terrain deposits later in this paper.

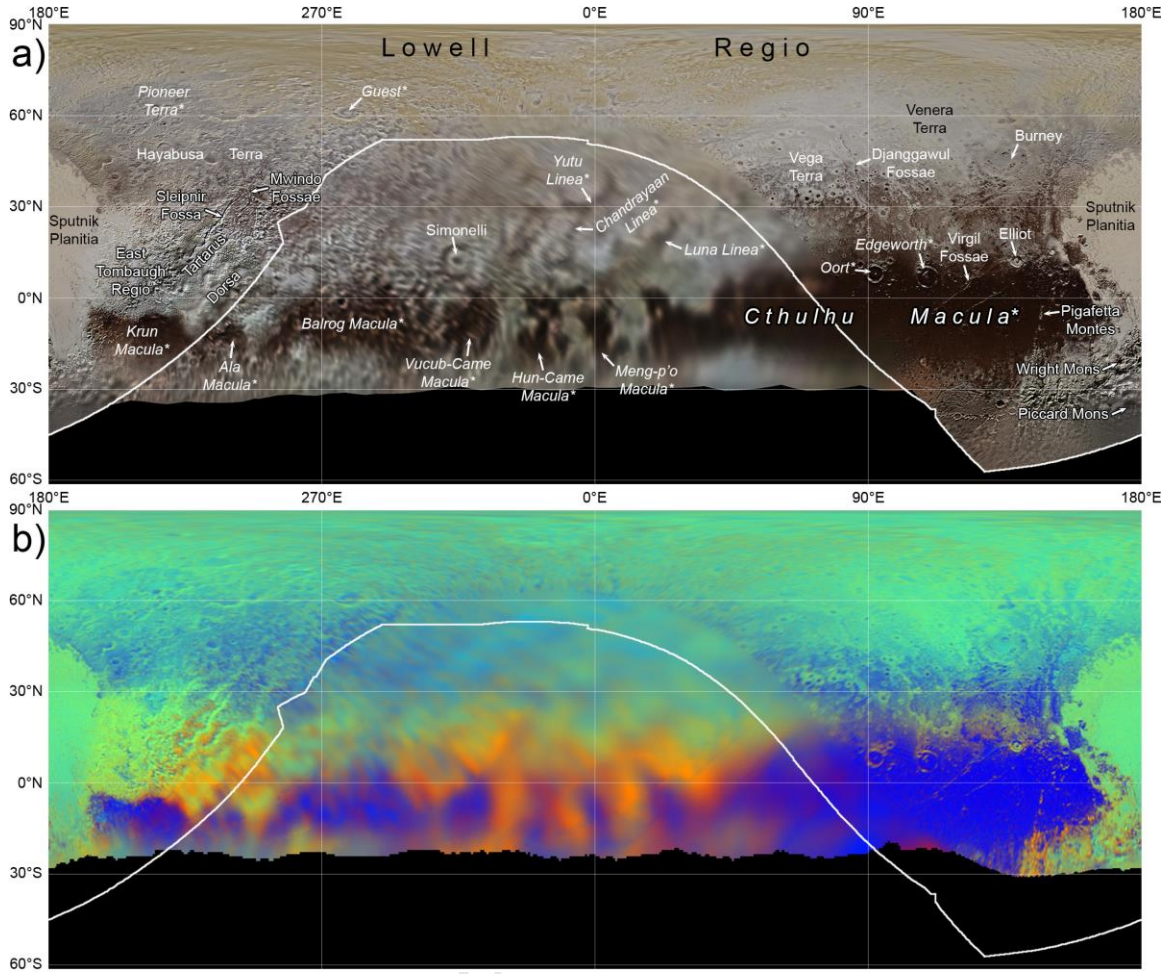

Figure 4. (a) A global, cylindrically projected image mosaic of Pluto produced at 300 m/pixel overlain by MVIC color data produced at 650 m/pixel (from Schenk et al. 2018). "Blue," "red," and "CH_4" MVIC filters were used to provide the greatest color contrast. Labels indicate both formally and informally named features referenced in the text: formal names are shown in regular font, whereas presently informal names are italicized and asterisked. (b) Same image mosaic overlain on a mosaic derived from MVIC observations showing the equivalent width of the 890 nm CH_4 absorption band (from Moore et al. 2018). Warmer colors indicate greater CH_4 absorption and hence greater CH_4 abundance. As in Figure 2, the white line on both maps here indicates the boundary of near side imaging.

3. Geological Mapping

The great contrast in pixel scale between New Horizons near side and the far side datasets means that contact definition and unit characterization for the FS must be based primarily on albedo variations seen in low-phase approach imaging, somewhat aided by interpretation from higher resolution NS images. At the pixel scale of the FS imagery, which ranges from 2.2 km/pixel to 41 km/pixel, only surface features on a scale larger than ≈10 km (at the western extreme of the FS) and ≈200 km (at the eastern FS extreme) are well-resolved. Detailed surface textures that are apparent in near side hemisphere imaging of <1 km/pixel are invisible on the FS.

Given the inability to observe detailed surface textures directly on the far side, near side imaging that abuts the far side is an important anchor for FS mapping. In this way, unit contacts and large-scale structures that are easily defined in high resolution NS hemisphere coverage can be interpreted into the FS. Further, though the digital elevation model created for Pluto (Schenk et al. 2018) does not extend into the FS, far side topography can be gleaned from examination of the terminator in FS approach imaging of pixel scale ~5 km/pixel or better. And in addition, limb profiles, even though they are sporadically distributed, allow us to assess topography on a scale of kilometers in some places on the FS. These limb profiles represent an invaluable resource for unit definition that supplement visible and color imaging; see Appendix A on topographic knowledge for further details.

Our FS geological mapping follows standard US Geological Survey (USGS) mapping protocol (Skinner et al. 2018) and is shown in Figure 5. Here we describe each of the mapped units and explains our mapping rationale.

Based on the continuations of albedo, color, and spectral units in the base maps in Figures 1-4, we find most of the FS units to also be represented in the near side hemisphere to some degree, and so we include descriptions of their appearance in near side imaging as well where appropriate. We now discuss each FS unit type that we have identified.

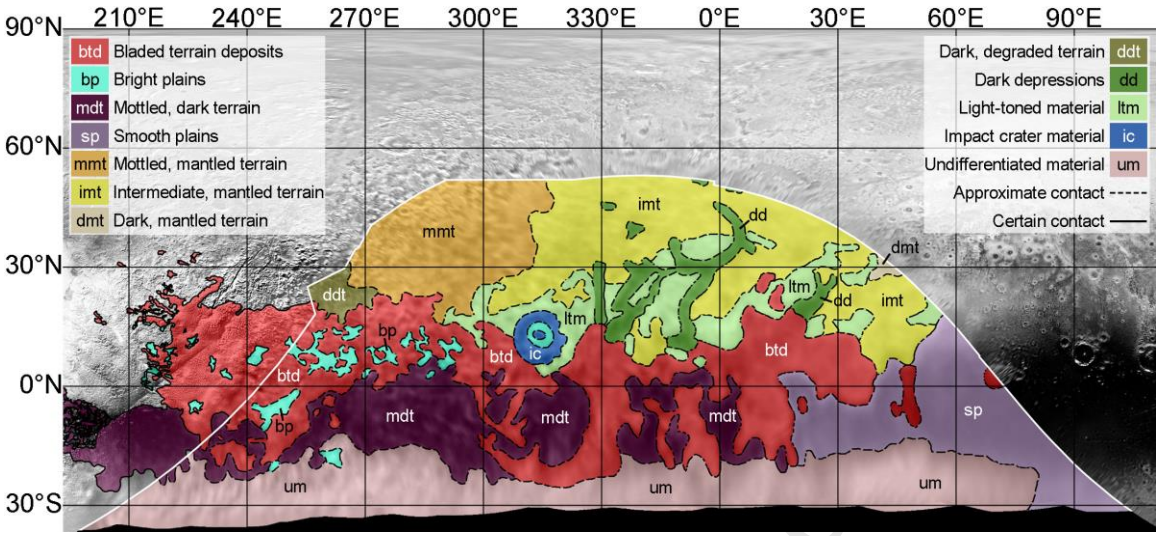

Figure 5. Geological map of Pluto's far side showing units identified by analysis of New Horizons imaging, spectral, and limb topography data. This map is overlain on photometrically equilibrated LORRI imaging ranging in pixel scale from 2.2 km/pixel (at the western boundary) to 40.6 km/pixel (at the eastern boundary), and surrounded by higher resolution, NS imaging. Given the low resolution of imaging covering Pluto's far side, all far side boundary contacts are treated as approximate. The white line here marks the imaging boundary of the FS. Near side geological mapping of Tartarus Dorsa and Krun Macula is included to the west of this boundary to represent continuations of FS units *btd*, *bp*, and *mdt*; adapted from Figure 2 in Moore et al. (2018).

Bladed terrain deposits (unit btd): This unit was originally identified at the eastern boundary of the near side hemisphere (Moore et al. 2016, 2018; Moores et al. 2017), where it forms high-elevation (reaching >4.5 km above Pluto's mean radius), elongated, sub-parallel swells or plateaus (Tartarus Dorsa) that can display relief of more than 3 km above the plains to its north. The surface of these swells has a unique texture consisting of dense fields of typically sub-parallel sets of steep ridges that are characterized by sharp crests and divides, referred to as "bladed terrain" (see Figure 6a). The blades are typically spaced 3 to 7 km crest-to-crest, and exhibit relief of ~300 m from crest to base. Spectral data from New Horizons (Grundy et al. 2016; Protopapa et al. 2017; Schmitt et al. 2017) indicate that the bladed terrain deposits are composed primarily of methane ice (see Figure 4b). Moore et al. (2018) interpreted these massive deposits as having precipitated at high elevation and low latitude during an era in Pluto's history when climatic

atmospheric conditions favored this formation scenario, with subsequent excursions in climate causing the deposits to partially sublimate and hence erode into the blades seen today. Later volatile transport modeling reproduced this formation scenario for these cold-trapped CH_4 deposits in Pluto's equatorial regions (Bertrand et al. 2019).

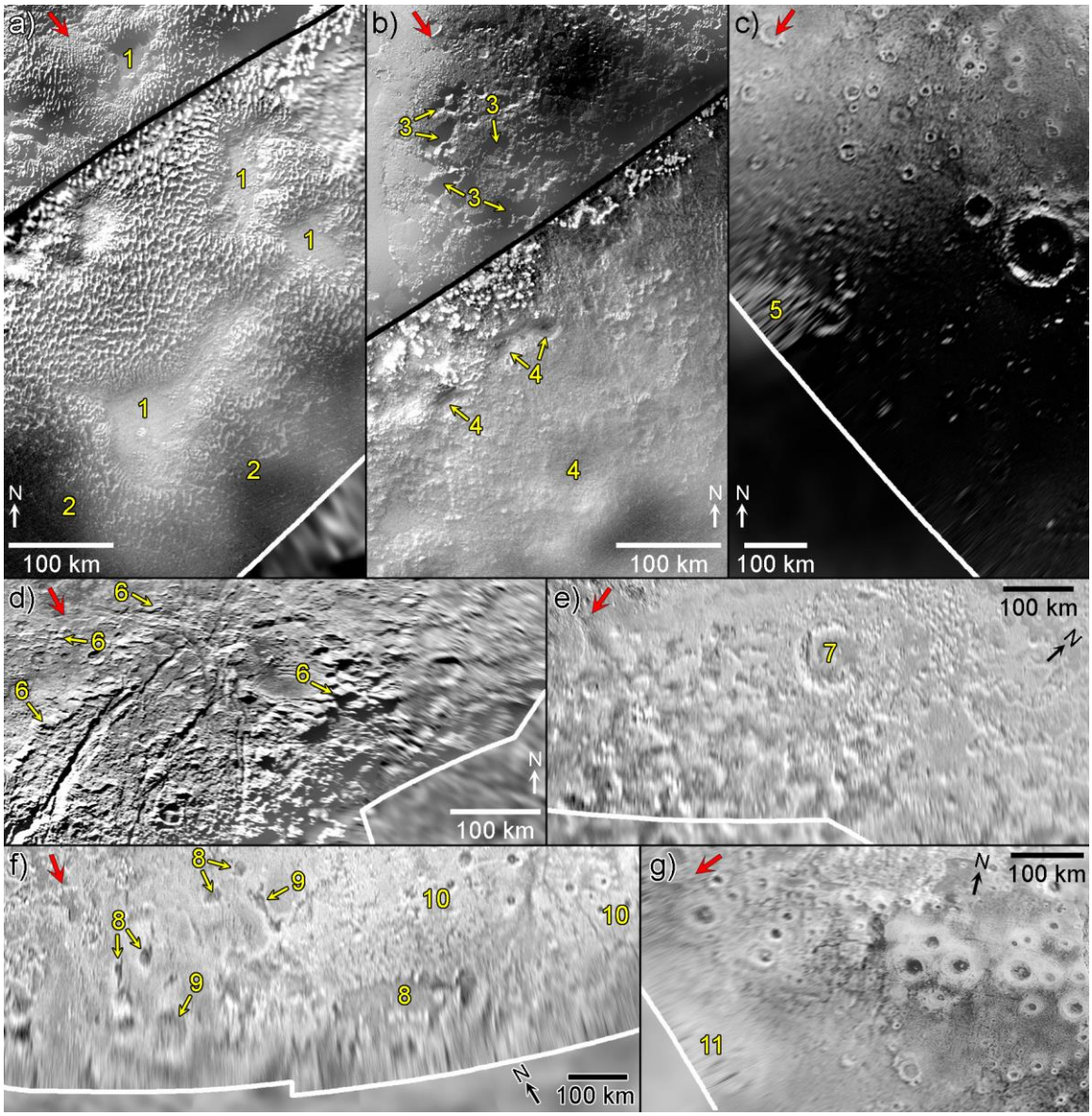

Figure 6. Various terrains within the near side hemisphere that border, and which are interpreted to form like geological units within Pluto's FS. Black lines indicate in panels the boundary between the directly illuminated portion of the NS hemisphere, and the haze-lit portion of the FS. Thick white lines indicate the boundary between the NS hemisphere and FS. Red arrows indicate illumination direction. Panel (a): Bladed

terrain deposits of Tartarus Dorsa (unit *btd*). Labels with a '1' indicate deposits of bright, volatile ices (unit *bp*) ponded on the floors of depressions amongst the dorsa. '2' labels indicate the gradational contact between Tartarus Dorsa and Krun Macula (lower left) and Ala Macula (lower right). Image is centered at 4.1°N, 228.8°E. Panel (b): Dark, eroded material of Krun Macula (above black line), which may be representative of unit *mdt*, and intermediate albedo, knobby terrain (below black line) that may be representative of unit *um* (at least its western region). '3' labels indicate large collapse pits within Krun Macula, and '4' labels indicate rimless, dark-floored depressions (or 'cavi'). This image is centered at 17.8°S, 198.4°E. Panel (c): Smooth, cratered plains (unit *sp*), with the plains in the lower half of the image displaying a veneer of dark haze particles or other darkening agents (e.g., charged particle radiolysis-, or UV irradiation produced) in Cthulhu and other maculae. '5' label indicates an expanse of bladed terrain deposits superposing the smooth plains. Image is centered at 4.5°N, 82.0°E. Panel (d): Dark, degraded terrain (unit *ddt*) in the vicinity of Mwindo Fossae. '6' labels highlight occurrences of jagged, hilly terrain with a distinctly arcuate morphology. This image is centered at 31.0°N, 250.1°E. Panel (e): Mottled terrain interpreted as a thick, light-toned mantling deposit partly covering a darker substrate (unit *mmt*). '7' label indicates an impact crater with the mantle partly covering its floor. This image is centered at 57.5°N, 282.5°E. Panel (f): The intermediate, mantled terrain (unit *imt*). '8' labels indicate isolated, dark floored pits that are likely smaller versions of the northern dark depressions seen in the far side (unit *dd*). This area marks a transition to a brighter, tectonized/mantled terrain ('10' labels). '9' labels indicate pits with high albedo material characteristic of this bright, mantled terrain occurring around their rims. Albedo contrast has been stretched in this image. This image is centered at 59.2°N, 4.5°E. Panel (g): Mottled terrain interpreted as a light-toned mantling deposit that is undergoing erosion to reveal a darker substrate (unit *dmt*). Bright-rimmed ("halo") craters occur frequently. '11' label indicates an especially bright region that may represent the light-toned material (unit *ltm*). This image is centered at 31.6°N, 69.8°E.

Bladed terrain deposits can be traced eastwards from the limit of their coverage in the haze-lit portion of the near side hemisphere. In low phase imaging, bladed terrain deposits appear as a low- to

intermediate-albedo unit that contrasts significantly with the bright plains and expanses of dark terrain (termed "maculae") in the equatorial zone. In the western FS, the sub-parallel Tartarus Dorsa transition to a less ordered configuration, with the bladed terrain deposits surrounding expanses of bright plains (unit *bp*, see below), and also occurring as outcrops several tens of kilometers wide within these plains. East of 320°E, the bladed terrain deposits appear as irregular and angular formations hundreds of kilometers across that intersperse with dark equatorial maculae and separate these maculae from lighter toned terrain to the north.

In this eastern region of the FS, MVIC color observations and limb profiles are crucial to the identification of these formations as bladed terrain deposits. We have found these correlate well to regions of high CH_4 absorption as shown in Figure 4b, and that limb profiles that cross these formations (see Appendix A Figure A1) indicate that they display relief of 2 to 4 km above adjacent terrain, which is similar to that of Tartarus Dorsa. The unit also shares a similar latitude range as Tartarus Dorsa, being located within 30° of Pluto's equator. Isolated outcrops of this unit in the far east of the far side are too small to be resolved in available spectral data, but are identified in limb topography. The easternmost outcrop of all, located at 70°E, 4°N, actually extends into the near side hemisphere. These FS observations indicate that Tartarus Dorsa forms the western extreme of a vast belt of bladed terrain deposits extending across the planet, within an equatorial zone spanning >220° of longitude, primarily on the FS. The only major gap in this distribution is around Cthulhu and Sputnik, i.e., between longitudes 75° and 210°E.

Bright plains (unit bp): Like the bladed terrain deposits, this unit was also identified via a combination of geological and color/compositional mapping of the eastern near side hemisphere (Moore et al. 2018). This unit appears as bright, generally smooth plains that occur on the floors of basins within East Tombaugh Regio and Tartarus Dorsa. This unit also displays a lightly pitted texture, with pits reaching down to <1 km in diameter. It extends into the western FS, where it appears as bright terrain (with the highest albedo of any imaged far side unit) that forms irregular and angular expanses that occur interstitially to the bladed terrain deposits, and which can also embay outcrops of the deposits.

The areal coverage of the unit decreases and becomes more sporadic with increasing longitude in low-phase, LORRI approach imaging

The *bp* unit is interpreted as ponded volatile ices, specifically a solid solution of N_2 ice and CO with trace amounts of CH_4 (Stern et al. 2015; Grundy et al. 2016; Protopapa et al. 2017; Schmitt et al. 2017) that have collected in depressions among the bladed terrain deposits. Precisely how far eastward the *bp* unit extends is unclear owing to resolution effects. However, the poorly defined *ltm* unit may partially consist of sub-resolution deposits of N_2-ice, but we note there is also compositional evidence for an eastwardly decreasing abundance of volatile ices, arguing against *bp* being very important here.

This unit forms a consistent veneer across the whole landscape in East Tombaugh Regio and is seen to pond in depressions there, but the veneer dissipates at around 220°E, and coverage in the western far side is limited to ponded deposits in such depressions. The main sequence of bright, volatile ice deposits terminates at ~290°E, but the floor of Simonelli crater (unit *ic*) at 315°E is also seen to display a high albedo, surrounding a dark central peak. Given that the ~250 km diameter Simonelli exists at the same latitude (12°N) as the well-resolved, 85 km diameter, central peak crater Elliot, located in the far east of Cthulhu Macula, which also displays bright deposits of volatile ices on its floor, it is reasonable to suspect that Simonelli's floor is also covered by such ice deposits, and we have mapped it as such. These inferences are consistent with the west to east surficial compositional sequence described by Moore et al. (2018), from dominance by nitrogen ice closest to the low elevation Sputnik Planitia, to the increasing dominance of methane ice to the east, culminating in the high elevation bladed terrain deposits.

Mottled, dark terrain (unit mdt): A dark, red, occasionally interrupted equatorial band of maculae extends around nearly the entire circumference of Pluto. This band is mostly contained within the permanent diurnal zone (Binzel et al. 2017) extending between latitudes within 13° of Pluto's equator. The cause of the low albedo has been interpreted to be a blanket of atmospheric haze particles that has accumulated on these surfaces (Moore et al. 2016; Gladstone et al. 2016; Grundy et al. 2016; 2018), but it could also be in part or wholly

produced by charged particle radiolysis or UV exposure (Grundy et al. 2016, 2018; Stern et al. 2018). Once established as an inert, dark mantling deposit, the blanket would generally be kept warm enough by the diurnal Sun to prevent it from becoming a cold trap for condensation of bright, volatile ices (Binzel et al. 2017; Earle et al. 2018a). Conditions at high elevation and on seasonally shaded slopes within this band, however, are apparently suitable for the deposition of CH_4 ice onto this dark blanket. This is manifested by the bladed terrain deposits that dominate elevated equatorial regions in the FS, as well as the CH_4-capped summit regions of Pigafetta Montes and north-facing slopes of nearby crater walls in eastern Cthulhu Macula (Bertrand & Forget 2019). Later, we discuss the hypothesis that brighter areas of the wispy terrain within some of these maculae represent seasonal volatile deposits in these regions that expose the dark macula substrate when seasonally removed to higher latitudes.

Surface features underneath this blanket often appear sharp and well-defined in imaging ranging from 76 to 890 m/pixel, meaning that the dark blanket of material is not thick enough to mask or soften topographic relief on a scale of hundreds of meters to kilometers, and its topographic signatures of individual geologic units are thus preserved. Grundy et al. (2018) estimated that unperturbed particle accumulation due to haze sedimentation would coat the surface to a thickness of ~14 m over the age of the solar system, consistent with this masking effect being below the resolution of New Horizons imaging. Ice radiolysis and UV-derived darkening rates have not been computed for comparison in the post flyby era.

The FS portion of this band of maculae extends from Krun Macula at 225°E to Cthulhu Macula at 80°E. From west to east, these are Ala, Balrog, Vucub-Came, Hun-Came, and Meng-p'o Maculae (see Figure 4a). The dark mantling deposit is not itself a geological unit, but covers a great variety of different terrains. NS imaging shows that Krun and Cthulhu Maculae are very different geologically. Krun consists of a rough upland plateau with interconnected complexes of pits, troughs, and basins up to 3 km deep and 20 km wide (Howard et al. 2017; Moore et al. 2018), indicating that widespread surface collapse has affected this terrain ('3' labels in Figure 6b). A few ($\lesssim$10) recognizable impact craters exist there, all of which are less than 20 km in diameter (Robbins

et al. 2017; Singer et al. 2019). Cthulhu however consists of km-scale smooth, cratered plains that are crossed by tectonic belts, and which are more heavily cratered than Krun Macula, with craters up to >100 km across (Robbins et al. 2017; Singer et al. 2019). The dichotomy between Krun and Cthulhu indicates that there must be at least one geological transition within the intervening chain of far side maculae. Such a transition is identified in the region between ~335°E and ~10°E (see Figure 4a), encompassing Hun-Came and Meng-p'o Maculae, which are surrounded to the east and west by large expanses of bladed terrain deposits. The maculae to the west of this longitude range (Balrog and Vucub-Came) present a mottled, wispy appearance at a scale of tens of kilometers (unit *mdt*), whereas the western extreme of Cthulhu Macula to the east appears homogeneous by comparison. This differing texture is not an artifact due to degrading resolution with increasing longitude, as the difference is apparent in approach images with consistent resolution from west to east. Besides Cthulhu Macula, Hun-Came and Meng-p'o Maculae are the only far side maculae that are crossed by limb profiles (see profiles C and D in Appendix A Figure A1). As seen in these limb profiles, these maculae are always depressed relative to the adjacent bladed terrain deposits, but to differing degrees: those within profile C appear to be more elevated with respect to the bladed terrain deposits than those within profile D, although this may be at least in part be due to off-limb topography obscuring their total topographic relief.

The close spatial association of the mottled, dark terrain to the bladed terrain deposits, and its tentatively identified higher elevation relative to Cthulhu Macula, suggest that a genetic relationship between the mottled, dark terrain and the bladed terrain deposits may exist. The mottled texture of the unit could represent poorly resolved outcrops of lighter-toned bladed terrain protruding above the dark blanket of haze (or radiolysis or UV exposure derived) particles, or alternatively, the remnants of seasonal deposits of CH_4 that have deposited at elevated and topographically prominent locations on top of the dark blanket (as at Pigafetta Montes). Section 5 includes further discussion of hypotheses to explain the characteristics of this unit.

Smooth plains (unit sp): At the western edge of the NS hemisphere, terrain south of ~30°N is occupied by cratered plains (see Figure 6c)

that are crossed by tectonic systems including Djanggawul and Virgil Fossae. These plains display a dark cover between ~13°N and ~23°S, and as noted previously, this cover has no discernable effect on the topographic relief of underlying landforms at the pixel scale of the imaging here (890 m/pixel). The dark equatorial plains and intermediate albedo plains on either side of them to the north and south can therefore be regarded as a single unit. On the FS, Cthulhu Macula appears as an expanse of homogeneous, dark terrain. The contact separating the northern, intermediate albedo plains from terrain to the north (the brighter intermediate mantled terrain and light-toned material, units *imt* and *ltm*) can be traced southwestwards, tapering until it meets the eastern limit of unit *btd* at ~40°E. Intermediate albedo plains are not identified west of 30°E, where the unit is only expressed as dark terrain bounded to the north by the bladed terrain deposits, and to the south by the undifferentiated material. An expanse of bladed terrain deposits separates the smooth plains from the irregular and angular Hun-Came and Meng-p'o Maculae located between 330°E and 20°E to the west, which we interpret to be occurrences of the mottled dark terrain. Limb profiles confirm that bladed terrain deposits are elevated above the smooth plains by a few kilometers (Appendix A Figure A1), with the former interpreted as being superimposed upon the latter. This can be observed directly just short of the limb in near side hemisphere imaging ('5' label in Figure 6c). Since these scattered, intermediate albedo bladed terrain deposits were likely emplaced onto higher portions of the cratered, darkened plains early in Pluto's history, they have experienced sufficient resurfacing via mobilization of the CH_4 ice to avoid being entirely mantled by the dark particles (in contrast to the lower elevation plains surrounding them).

Dark, degraded terrain (unit ddt): In 890 m/pixel NS imaging obtained at high phase (solar incidence >80°), terrain in the vicinity of the radial tectonic features Mwindo Fossae displays flat plains interspersed with jagged and degraded hills that have a somewhat arcuate (i.e., curvilinear ridges with steep south-facing and gentle north-facing slopes) morphology (Moore et al. 2018) ('6' labels in Figure 6d). In low phase approach imaging, this same terrain appears dark relative to surrounding terrain, and extends into the far side to the east of Mwindo Fossae. Geological mapping (Moore et al. 2018) indicates that the arcuate terrain underlies the bladed terrain deposits, and it was

suggested there that a genetic relationship exists between the two units, with the arcuate terrain possibly being marginal deposits left behind after retreat of more extensive bladed terrain deposits. The dark, degraded terrain may therefore represent ancient water ice crust that was previously covered by the bladed terrain deposits prior to their recession, and which could have extended north as far as the southern limit of the mantled terrains (30°N-40°N).

Mottled, mantled terrain (unit mmt): Across all longitudes, the northern latitudes of Pluto differ from the equatorial regions in that they display a conspicuously homogeneous and intermediate albedo compared to the strong albedo contrasts exhibited by the equatorial regions, as manifested most obviously in the dark maculae and the bright Tombaugh Regio. This albedo difference has been attributed to the fact that the high latitudes have experienced more extreme insolation variation and seasonal cycles during Pluto's history, which should result in considerable and even ongoing volatile exchange in response to such cycles, and which should be recorded to some extent in Arctic landscapes (Bertrand & Forget 2016; Binzel et al. 2017; Earle et al. 2018a). This response is in contrast to the equatorial regions, where temperature modeling calculations show that consistent diurnal variations are effective in enhancing runaway surface albedo variation, and for long-term preservation of whatever material is "seeded" there (Binzel et al. 2017; Earle et al. 2017; Bertrand et al. 2020). There, evolution of landscapes subject to modification by exogenic processes would instead tend to reflect secular, irreversible changes in Pluto's climate (Moore et al. 2018).

The NS area to the northeast of Sputnik Planitia is also characterized by rounded terrain that is smooth-textured on a scale of a few kilometers, mapped as "smooth uplands" by Howard et al. (2017), and displays a CH_4 spectral signature. This morphology is diagnostic of accrescence, whereby deposition of a thick mantle has occurred uniformly over a regional surface, causing projections to become rounded and inward facing, and valleys to become sharply indented. East of ~260°E, this mantled terrain takes on a mottled appearance, with the lighter-toned mantling deposit forming irregular, lobate, flat-topped plateaus that are separated by lower albedo depressions, their lower elevation resolved by the topographic mapping of Schenk et al. (2018) (see Figure 6e).

Notice that this NS terrain continues eastward into the FS, where it is mapped as mottled, mantled terrain (unit *mmt*), as far as 310 to 320°E. We interpret the lobate appearance of the plateaus to also be an accrescence texture, implying that this unit is where mantling of the surface has occurred to an incomplete degree, leaving gaps where the darker substrate remains exposed. At 61°N, 278°E, the mantle partly in-fills the 115 km diameter Guest impact crater ('7' label in Figure 6e). Howard et al. (2017) mapped an expanse of low albedo "eroded, smooth plains" on the NS within Hayabusa Terra to the south of the brighter, thickly mantled smooth uplands, and the mottled, mantled terrain, which appears to display characteristics of both these terrains and may record a history of alternating deposition and erosion (the latter occurring at least in part due to sublimation) of the mantling material.

Intermediate, mantled terrain (unit imt): Tracing the northern boundary between the near side hemisphere and the far side, the mottled, mantled terrain transitions at ~310-320°E to a terrain where the dark-floored depressions are far fewer, not connected, and sporadically distributed ('8' and '9' labels in Figure 6f). This appears to indicate that coverage by the mantling deposit is generally more consistent and complete here than in the mottled, mantled terrain. As such, FS terrain at this location has been mapped as intermediate, mantled terrain (unit *imt*). Given the low resolution of the far side central and eastern regions (>15 km/pixel), we have designated most of the intermediate albedo terrain to the east as belonging to this unit, as no contacts can be identified within it.

Whereas this unit appears as a relatively consistent mantling deposit where it occurs at the boundary between the near side hemisphere and the far side, more generally we regard this unit as representing northern mid-latitude terrains (i.e. mostly north of ~15°N) that are variably mantled by predominantly CH_4 ice-rich material (Grundy et al. 2016; Protopapa et al. 2017; Schmitt et al. 2017; Earle et al. 2018b; Bertrand et al. 2019), but which nevertheless show a fairly consistent intermediate albedo.

We also note that the northwest of the near side hemisphere displays a mantling deposit ('10' labels in Figure 6f) that has a higher albedo than the intermediate mantled terrain, is tectonized and partly eroded, and

also shows impact craters with generally sharply defined rims and dark floors. This represents an extension of the "fretted terrain" of Vega and Venera Terrae, described by Moore et al. (2016). Due to the particularly low resolution of far side imaging in this area, and the subtle difference in shading between this unit and the intermediate mantled terrain, it is difficult to determine if this bright mantling deposit extends into the far side at all, but we have not mapped it as doing so. Within the near side hemisphere, these two mantling deposits appear to make contact in the region around 62°N, 357°E, where the bright, mantled terrain lines the rims of the easternmost dark pits of the intermediate mantled terrain ('9' labels in Figure 6f). The near side intermediate albedo, mid-latitude, mantled terrains of Vega and Venera Terrae display a high crater count (Robbins et al. 2017; Singer et al. 2019) that extends to the boundary with the far side, and it is reasonable to assume that unit *imt* is cratered to a similar degree.

Dark, mantled terrain (unit dmt): Within the western near side hemisphere, in Vega Terra, there is a mid-latitude, generally low albedo zone that has a mottled appearance on a scale of a few kilometers (in 232 m/pixel imaging). This zone seems to be where overlying, higher albedo material (possibly the material of the bright, mantled terrain to the north, or material of the smooth plains to the south) is undergoing degradation and removal, leaving darker material exposed underneath, which may be haze or radiolysis-/UV exposure-derived particles that have settled in depressions. The mottled texture continues eastwards as a mid-latitude band as far as Sputnik Planitia. Vega Terra also features prominent "bright-halo craters," which display conspicuously bright inner and outer walls, and dark floors (Moore et al. 2016) (see Figure 6g). To the west, this terrain can be discerned on the far side as an especially low albedo promontory (the dark, mantled terrain, unit *dmt*) extending into the intermediate, mantled terrain; however, it does not appear to extend very far into the far side (<150 km), although the very low resolution of the imaging here makes its true extent difficult to determine.

Light-toned material (unit ltm): In the FS northern low- to mid-latitudes there is a roughly defined band of light-toned material (unit *ltm*) that is brighter than units contacting it (specifically the bladed terrain deposits, intermediate, mantled terrain, and dark depressions), but is also not as

bright as the volatile ice of the bright plains. This is our most tenuously defined far side unit. It borders our mapping area at a few locations in the far east, and we consider a particularly bright region here (label '11' in Figure 6g) to be what is perhaps its only representation in the near side hemisphere, although the imaging here is very oblique. It also bounds the dark depressions (unit *dd*), relative to which it is elevated, and also the bladed terrain deposits (unit *btd*), relative to which it is depressed. As indicated in profile A of Appendix A, Figure A1, where the unit borders the eastern edge of the far side, it appears to be topographically prominent relative to surrounding terrain. This suggests that at least some portions of the light-toned material may indicate seasonal deposits of bright CH_4 ice as observed at Pigafetta Montes and in the bright halo craters (Moore et al. 2016, 2018), forming a thin, discontinuous veneer that is covering the mottled, mantled terrain (unit *mmt*) and the intermediate, mantled terrain (unit *imt*). Becasue *New Horizons* observed Pluto during the northern spring, this might mean that these deposits represent CH_4 ice that has been freshly deposited during the northern winter/spring (Bertrand & Forget 2019). Yet in profile B of Appendix A Figure A1, the unit tends to be depressed relative to adjacent units including *btd* and *imt*, and even though the unit is not obviously sequestered within large depressions like the bright plains-forming material (unit *bp*), it therefore cannot be discounted that bright volatile ice that has deposited within depressions that are too small to be resolved by the imaging in this part of the far side (>10 km/pixel) may also partly contribute to the high albedo of this unit.

Dark depressions (unit dd): The dark depressions present the lowest albedo of any FS unit within northern mid-latitudes, and mainly cluster in a 40° wide zone of longitude between 330°E and 10°E. Here, they appear as lineations that reach hundreds of kilometers long and tens of kilometers wide, and extend north from the bladed terrain deposits. The morphologies of these lineations range from linear to sinuous (Chandrayaan Linea) to crescent-shaped. (Yutu Linea). Luna Linea has been mapped as extending from the bladed terrain deposits at 20°E.

Our recognition of the lineations as depressions is based on a backlit 800 m/pixel LORRI limb observation (see Figure 7), in which the haze layers extending above the limb are sufficiently bright such that

foreground depressions are dimly illuminated by forward scattering. The limb crosses Yutu Linea, and the section of the limb that coincides with this lineation (between the green arrows in the map in Figure 7A) appears to be at the crest (between the green arrows in the limb profile in Figure 7B) of a wider zone of elevated terrain that extends on either side of the lineation (between the orange arrows in Figures 7A and 7B). The location of the lineation within the LORRI frame, however, also corresponds to a 70 km-wide notch that extends below the limb (between the green arrows in Figure 7C), with a bright strip separating this notch from the limb itself. We interpret this to mean that the dark lineation represents a valley that is surrounded on both sides by elevated terrain: the off-limb eastern rim of the valley appears in the foreground of the LORRI frame as the notch, the off-limb western rim of the valley appears in the background and forms the section of the limb profile between the green arrows, and the bright feature represents illuminated atmospheric haze or cloud particles within the valley itself. Stern et al. (2017) identified this same feature as a possible low-lying cloud (relative to local topography), existing within a few km of the surface. Accordingly, we do not consider the dark lineation to represent an expanse of bladed terrain deposits, which are otherwise responsible for most of the elevated terrain seen within far side limb profiles, and are also apparent elsewhere within this same limb observation (bounded by red arrows in Figure 7). These deposits are located slightly off-limb (see Figure 7A) but their topographic relief is still high enough that they appear prominently in the limb profile (see Figure 7B). In contrast to the dark lineation in Figure 7C, no illuminated haze corresponding to a "hidden" depression is apparent below the limb for the bladed terrain deposits (see Figure 7D).

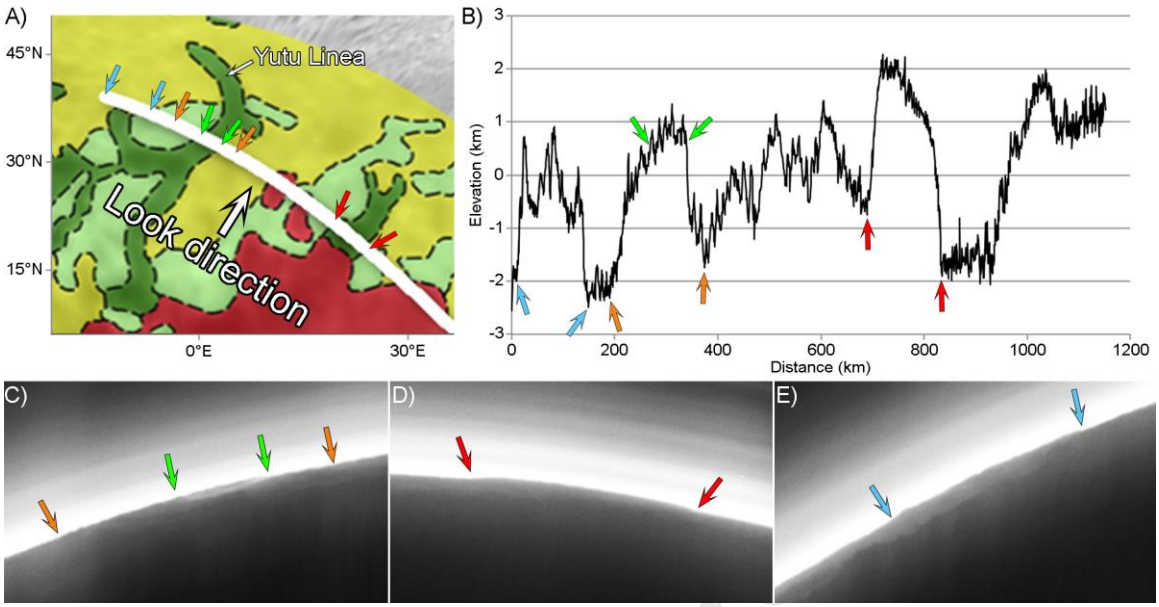

Figure 7. Topography appearing in an 800 m/pixel LORRI observation of Pluto's far side. (A) Detail of the geological map in Figure 5 with a segment of the limb ground track overlain. Colored arrows indicate the boundaries of topographic features seen in the limb profile and imaging in B-E. Look direction of the LORRI observation is indicated as shown by the white arrow. (B) The limb profile of the LORRI observation (the same as profile B in Appendix A, Figure A1), with colored arrows indicating the boundaries of various features. Blue arrows mark the boundary of a region of elevated terrain just north of the western end of Yutu Linea. Orange arrows mark the boundary of a region of elevated terrain that surrounds Yutu Linea. Green arrows mark the boundaries of Yutu Linea itself, which also coincide with the end points of the bright feature seen just below the limb in the LORRI image in (C). Red arrows mark the boundaries of an expanse of bladed terrain deposits. (C-E) Imaging from high phase (170°) LORRI observations, annotated with colored arrows that mark the locations of the same features on the limb as are shown in (A) and (B).

We interpret the depressions that form unit *dd* to be where the mantling material of the intermediate, mantled terrain has been removed, revealing a darker substrate. Different mechanisms have likely acted to remove the overlying mantle depending on location. In the case of Yutu Linea, we consider the evidence within the limb profile and its corresponding LORRI frame to indicate that it is a crescent-shaped valley with raised rims on either side. When seen in polar projection,

the crescent of Yutu Linea forms the arc of a circle, raising the possibility that Yutu Linea may indicate the presence of an impact crater there. Note that the limb in Figure 7 does not cross the western end of Yutu Linea, but rather terrain slightly to its north, which appears elevated in the limb profile (between the blue arrows in Figure 7) relative to terrain around it, similar to the elevated terrain that surrounds Yutu Linea to the east (between the orange arrows in Figure 7). This western, elevated terrain overlaps with where a circle formed from the continuation of Yutu Linea would lie, suggesting that such a circle forms an annulus of elevated terrain, i.e., which could be the rim of an impact basin ~350 km in diameter. In this scenario, such a basin would have been overlain by the mantling material of unit *imt*, coating its rim and infilling its floor. The crescent valley of Yutu Linea is where the mantling material is absent along the eastern and southern walls of the crater, perhaps due to it having been removed by sublimation erosion, but the mantle remains intact along the northwest rim of the crater. If this feature is a partially mantled impact basin, then Guest crater on the near side ('7' label in Figure 6e) may represent an analogue. Guest crater is 115 km in diameter and its floor is partially covered by mantling material of the *mmt* unit, with a crescent-shaped trough separating the floor deposits from the western rim of the crater.

The location and configuration of the network of linear and sinuous lineations of unit *dd* that extend between Yutu Linea and the bladed terrain deposits (which include Chandrayaan Linea) suggest that they have originated due to structural anisotropies in Pluto's crust. The concentration of these lineations between ~330°E and 0°E places them neatly in line with the NNE-SSW-aligned ridge-trough system that spans the entire near side hemisphere (Schenk et al. 2018), and if they are an extension of this system, then they would represent fracturing of Pluto's crust after deposition of the mantle. The oblique angle that some of the lineations make to the trend of this system, however, suggests that not all of them originate due to the same tectonic forces that produced it. Alternatively, the lineations, in addition to the irregular and angular bladed terrain deposits and maculae that occur immediately to the south of them, may instead represent a >1000 km diameter zone of crustal disruption that is located antipodal to the location of the Sputnik basin-forming impact. Such disruption (and accordingly the Sputnik impact) would have necessarily occurred after the deposition of the

mantle. The eastern outlier of Luna Linea may be a distal manifestation of the same phenomenon that formed the closely spaced network of lineations to the west, or it may be a depression that formed through unrelated means. See text below on possible tectonic and antipodal effects for further details.

The *dd* unit also includes a handful of northern, isolated, dark patches tens of kilometers across that are separated from the main cluster of lineations, which we interpret to be larger versions of the dark pits seen to the north within the intermediate, mantled terrain of the near side ('8' and '9' labels in Figure 6f), a few of which border the far side. The margins of these depressions are resolved to have a jagged, angular outline in 890 m/pixel imaging. Such morphology is characteristic of decrescence, i.e., uniform removal of material from a landscape (e.g. Howard & Selby 2009), suggesting that they have formed by sublimation erosion of the mantle.

Simonelli impact crater material (unit ic): The only unambiguous impact feature that has been identified on the FS is the ~250 km diameter featured named Simonelli, located at 12°N, 315°E (see Figure 8). Its status as a central peak crater is confirmed by low Sun terminator imaging, where its walls and central peak display clear evidence of a raised peak and annular rim (see Figure 8a). At higher solar illumination, Simonelli's walls and central peak appear dark, with a bright annulus separating them (see Figure 8b). This annulus is interpreted to volatile ices that have deposited onto its floor, similarly to the somewhat smaller, 85 km diameter Elliot crater in the near side hemisphere (see Figure 8c). Bordered by bladed terrain deposits to its south and located within an area that shows high methane absorption (see Figure 4b and Moore et al. (2018)), this impact may have occurred into the bladed terrain deposits or it may have been modified by the subsequent deposition of bladed terrain materials. Further details on Simonelli are discussed below in Section 5.

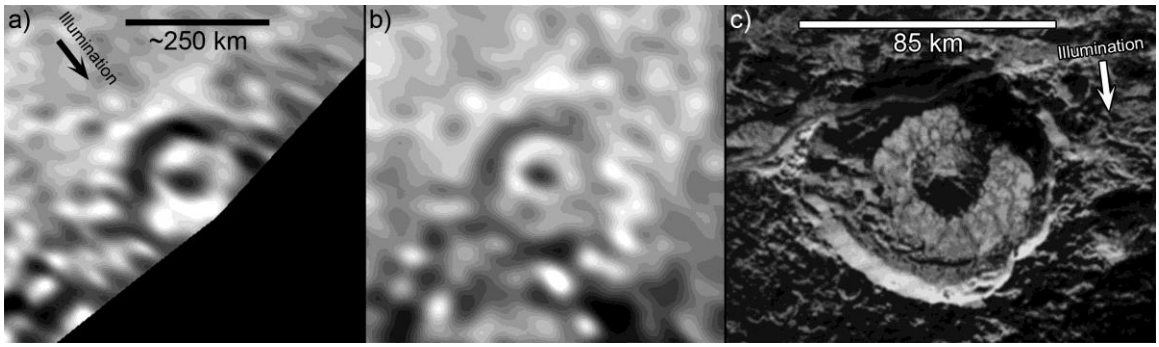

Figure 8. (a) Simonelli crater seen at nearly 90° phase in 9.3 km/pixel imaging, re-projected to cylindrical projection; illumination is from upper left. (b) Simonelli crater seen at nearly 0° phase angle in 16.9 km/pixel imaging, re-projected to cylindrical projection. (c) Elliot crater seen in 320 m/pixel imaging, with bright volatile ices condensed on its floor and surrounding its central peak.

Undifferentiated material (unit um): The region south of the dark equatorial band on the far side consistently appeared only as a narrow strip along the limb in approach imaging, and so was only viewed at very high emission angles (>80°). As such, it appears smeared when re-projected in the global mosaic, which in combination with the low resolution of the imaging, further confounds characterization of this region, to the extent that we have chosen to designate it as "undifferentiated material." The unit has an overall intermediate albedo, but also displays albedo contrasts that form a mottled texture on a scale of tens of kilometers, a texture that is tentatively identified as far east as 30°E, where there is a transition to lighter, more homogeneous terrain. In approach imaging, this intermediate albedo, mottled texture is also seen to characterize terrain south of Krun Macula within the near side hemisphere, and in 320 m/pixel haze-lit imaging it is seen to have a rubbly, knobby texture on a scale of several kilometers (see Figure 6b). There are no recognizable impact craters here (Robbins et al. 2017; Singer et al. 2019), although there are rimless depressions (termed cavi) that reach tens of kilometers across with dark deposits on their floors ('4' labels in Figure 6b). The presence of the cavi and the apparently youthful surface of this terrain suggest that it may be related to the tentatively cryovolcanic edifices Wright and Piccard Montes to the west (Moore et al. 2016; Schenk et al. 2018; Stern et al. 2018), although there are no constructional landforms here. This rubbly terrain likely continues eastwards into the far side to form at least the westernmost

portion of unit *um*, but the low quality of the imaging prevents any confident differentiation of this unit between 225°E and 50°E. There is also the possibility that bladed terrain deposits extend further south into this unit than has been mapped in Figure 5, but neither visible imaging nor spectral data (i.e., methane absorption, see Figure 4b) are available to confirm this conclusion. However, we do note that climate models suggests that the Bladed Terrain are currently not symmetric to the equator, but are instead more extended to the northern latitudes due to the hemispheric asymmetry in insolation controlled by the current orbital parameters (in particular the solar longitude of perihelion, Bertrand et al. 2019).

4. Possible Tectonic and Sputnik-Antipodal Effects on Pluto's Far Side

Mapping of Pluto's near side shows that Pluto possesses a global network of extensional faults (Stern et al. 2015, Moore et al. 2016, Keane et al., 2016, McGovern et al. 2019). The orientation of these faults is not random—they follow coherent patterns over large swaths of Pluto—likely hinting at a singular origin or perhaps only a few common origins. The current favored model for this tectonic pattern focuses on the formation of the Sputnik Planitia basin and glacier that dominates the NS of Pluto (Keane et al. 2016). The combination of glacier loading, true polar wander, and global expansion plausibly due to the freezing of a subsurface ocean (Hammond et al. 2016; Nimmo et al. 2016; Kamata et al. 2019) produces a generally reasonable fit to the observed tectonic pattern on Pluto's NS (Keane et al. 2016).

If this hypothesis is correct, these same tectonic stresses should extend to Pluto's FS as well, as the stresses from true polar wander and global expansion are inherently global. The loading of sufficiently large features like SP can also contribute to global stress patterns (e.g., Melosh 1980; Matsuyama et al. 2014). Figure 9 shows the predicted tectonic pattern from Keane et al. (2016). Higher stress areas correspond to areas more prone to tectonic fracture.

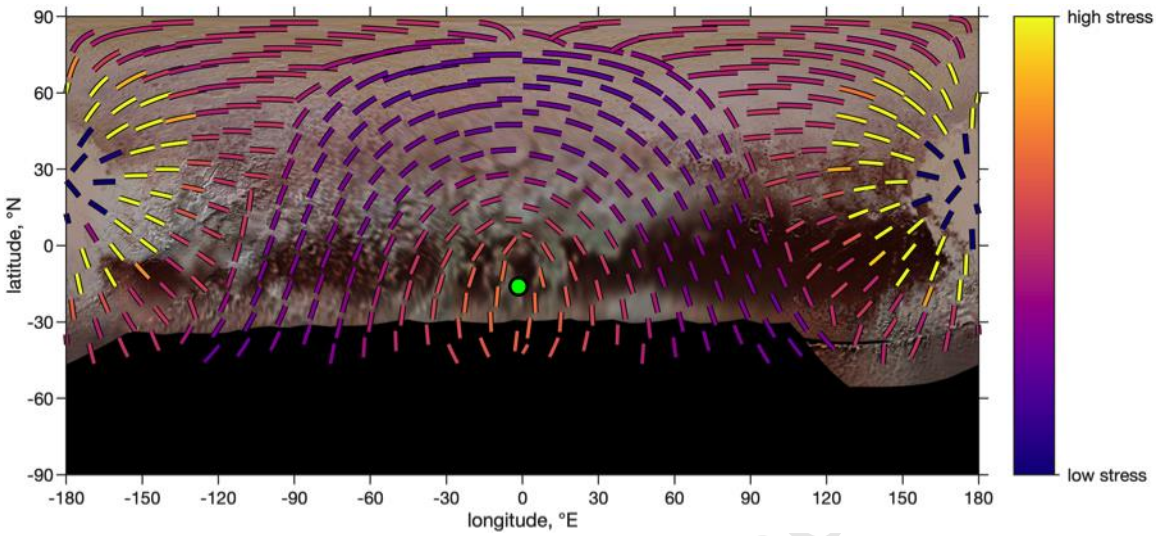

Figure 9: The predicted tectonic pattern on Pluto due to loading of the Sputnik Planitia glacier, true polar wander, and global expansion (from Keane et al. 2016). The line segments shown indicate the predicted orientation of extensional faults (i.e., graben); the color of each line segment corresponds to the mean calculated lithospheric stress. The magnitude of the stress depends on the extent of Pluto's global expansion, but is generally >1 MPa. Proximal to Sputnik Planitia, loading stresses dominate, producing faults that are quasi-radial to Sputnik Planitia. Distal to Sputnik Planitia, true polar wander stresses become dominant. The green circle indicates the location of the Sputnik Planitia antipode.

The predicted stresses on Pluto's FS are slightly lower than on the NS owing to the decreased contribution of loading stresses. However, near the Sputnik Planitia antipode (green circle in Fig. 9), these stresses are similar to the stresses predicted near major faults on the NS (e.g., Djanggawul, Virgil, and Sleipnir fossae). This antipodal region is associated with alternating, roughly north-south-aligned segments of the bladed terrain deposits (unit *btd*) and mottled, dark terrain (unit *mdt*) between 320°E and 20°E (incorporating Hun-Came and Meng-p'o Macula), consistent with the predicted orientation of extensional faults in this model. It is thus conceivable that these FS geologic features may be related to such tectonic origins.

While the Keane et al. (2016) model produces patterns that can replicate much of the observed near side tectonics, and which are suggestive of the surface markings in this antipodal region, this is not

true everywhere. One of the most dramatic physiographic features on Pluto's near side hemisphere, discovered in the topographic mapping of Schenk et al. (2018), is a complex, eroded, fragmentary band of graben, troughs, ridges, plateaus, tilted blocks, and elongated depressions (or 'cavi') that extends at least 3200 km from the north pole southward to the limit of coverage at ~45°S, and which is ~300 to 400 km wide. Designated by Schenk et al. (2018) as the "great north-south Ridge-Trough System" (RTS); this NNE-SSW-trending band crosses the equator at 150°E. Its configuration and global scale is suggestive of an origin stemming from a planetary-scale loading mechanism, and the landforms that compose it appear to derive from extensional tectonics. The most plausible scenario to generate a wide band of terrain with the required orientation of extension is equatorial thickening of the water ice shell lithosphere of Pluto (McGovern et al. 2019), in which case the RTS would represent a paleo-equator. Since the RTS now trends NNE-SSW, this would imply a truly dramatic amount of true polar wander of Pluto, an amount not predicted by the model of Keane et al. (2016).

If the RTS is global in extent, we can ask whether it is detectable in FS imaging. Schenk et al. (2018) identified several dark-floored depressions in the well-resolved polar region of Pluto's near side, and suggested that other dark, irregularly shaped features in the poorly-resolved portion of the FS may also be depressed, possibly indicating that the RTS trend continues to Pluto's far side but with a different, less linear character. We have mapped these dark features as unit *dd*. High-phase limb imaging confirms that they are depressions (see Figure 7), but a confounding factor is that, while the limb observation that crosses Yutu Linea is helpful in its interpretation, imaging limitations still prevent us from determining the precise nature and origin of the depressions in general, e.g., whether they are graben (like those seen in the polar portion of the RTS) or elongate cavi (like those seen in the equatorial portion of the RTS). Schenk et al. (2018) also noted that limb profiles in medium-resolution departure images indicate an unusually rugged topography near 320–340°W at ~30°N, which might also represent an extension of the northern section of the system.

We have extrapolated great circles of the faults of the NS RTS (Figure 10) to Pluto's FS (Figure 11). These show a concentration oriented along the 330°E meridian, antipodal to the 150°E alignment of the RTS in the

NS hemisphere. This concentration overlaps with the westernmost lineation of unit *dd*, aligned almost exactly along this meridian (see Figure 5), and also overlaps the NNE-SSW-oriented lineations of unit *dd* between 335° and 345°E, although the orientations of these lineations make an oblique angle to the great circles. However, occurrences of unit *dd* lying further eastward, including the large crescent-shaped Yutu Linea, Chandrayaan Linea, and the even farther removed Luna Linea, do not line up convincingly with RTS great-circle pathways.

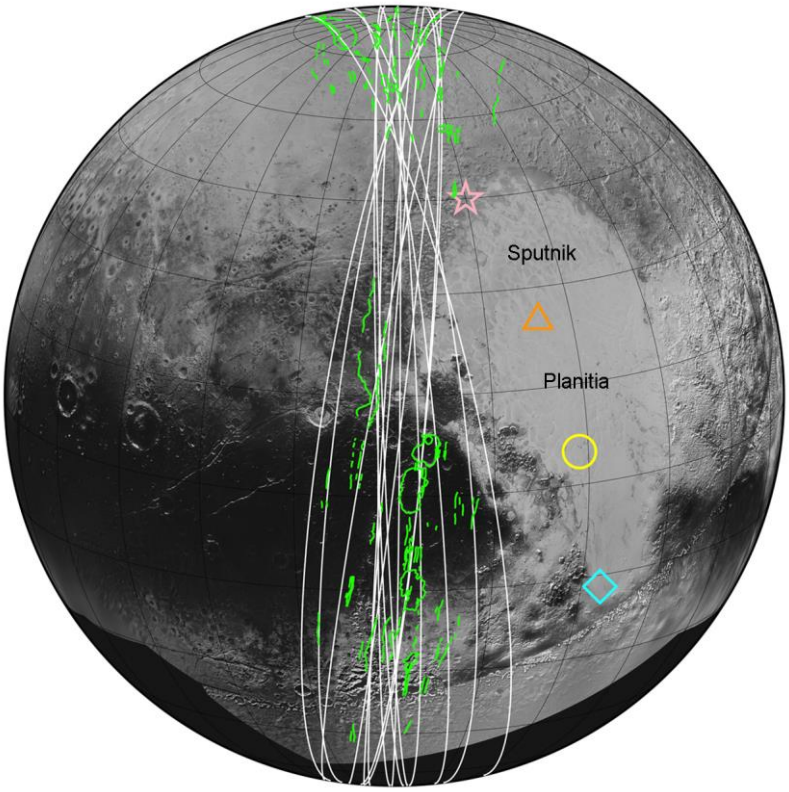

Figure 10. Spherical orthographic projection of the global mosaic shown in Figure 2, focusing on the near side hemisphere. Center of projection is 150°E, 15°N. The green lineations indicate the tectonic system dubbed the "great north-south ridge-trough system," or RTS (Schenk et al. 2018). The white lines represent great-circle paths fit to individual lineation segments of the RTS. The star, triangle, circle, and diamond symbols represent a potential first contact point for (i) an impact incidence from the NNW, (ii) the center of the deep portion of the Sputnik basin, (iii) a southern extension of SP basin-filling materials, and (iv) the potential first-contact point for an impact incidence from the SSE, respectively.

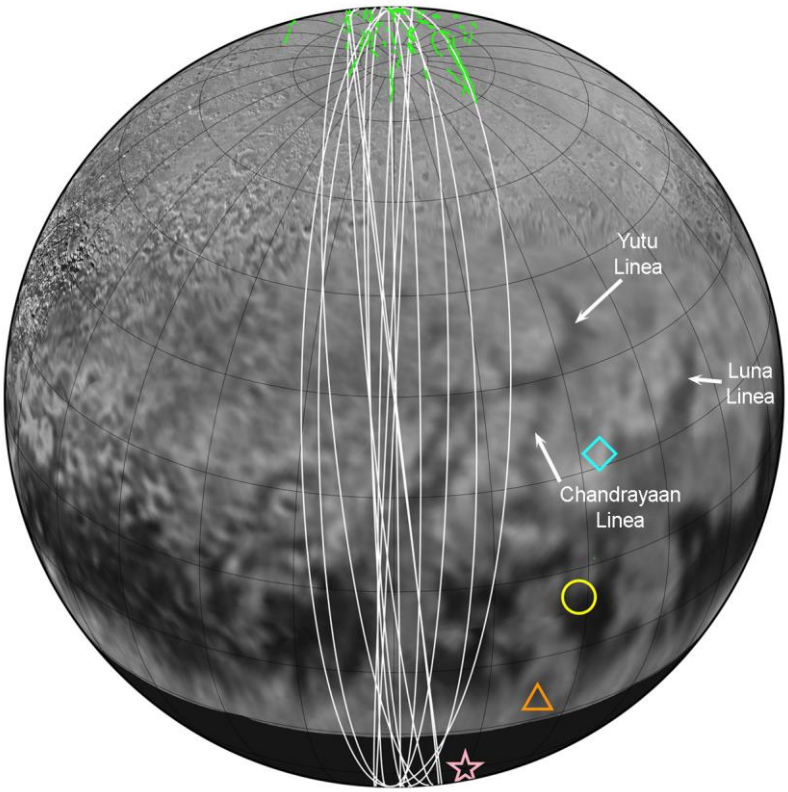

Figure 11. Global mosaic, as in Figure 10, but focusing on Pluto's far side. The center of projection here is at 330°E, 30°N. The star, triangle, circle and diamond symbols indicate the antipodes of those corresponding Sputnik basin-related locations in Figure 10.

Departures from the expected focus along the 330°E meridian and an essentially north-south alignment may be due to regional-to-hemispheric-scale variations in the structure of Pluto's ice shell and the stress field variations resulting from them, which could significantly perturb the tectonic stresses on the FS. Non-tectonic features like impact basin rims (possibly in the case of Yutu Linea) and flexural moats of central volcanic edifices could also account for the annular nature of some mapped structures. Further south, the north-south-aligned fabric of the RTS may account for the aforementioned alternating regions of N-S-trending bladed terrain deposits (unit *btd*) and mottled, dark terrain (unit *mdt*) between 320°E and 20°E. Because these particular patches of *mdt* are (i) lower than the surrounding *btd*; and (ii) elongate and broken up, in strong contrast to the more continuous or bulbous *mdt* units to the west, it is possible that the narrow, angular and roughly north-south aligned segments of *mdt*

between about 340°E and 10°E are southerly continuations of the *dd*/RTS trends.

Neither the configurations of the far side lineations of unit *dd* nor that of the near side RTS are consistent with the predicted tectonic pattern of Keane et al. (2016), suggesting that this tectonic model is incomplete. One possible solution to the conundrum is that the RTS may predate some aspects of the global tectonic pattern observed today (Schenk et al., 2018) and that Pluto may have experienced multiple episodes of true polar wander, reorientation, and tectonic activity over its history.

Another potential influence on the geology of Pluto's FS besides tectonism is the antipodal response of a catastrophic event occurring in the NS. In general, it is known that basin-forming impacts across the solar system can have major terrain-altering effects at locations antipodal to the point of impact, both from convergence of ejecta (Wieczorek & Zuber 2001) and also due to focusing of shockwaves traveling around solid planets (e.g., Schultz & Crawford 2011). The enormous depression that contains the massive nitrogen ice deposit of Sputnik Planitia has been interpreted to be an impact basin (Stern et al. 2015; Moore et al. 2016; McKinnon et al. 2016; Johnson et al. 2016; Keane et al. 2016; Nimmo et al. 2016; Schenk et al. 2018), in which case its elongated shape is suggestive of excavation by an oblique impact (McKinnon et al. 2016).

Elliptical and elongated craters are created by low-incidence-angle impacts (Elbeshausen et al. 2013); examples include the South Pole–Aitken impact basin on the Moon (e.g., Garrick-Bethell & Zuber 2009) and the Hellas impact basin on Mars (e.g., Andrews-Hanna et al. 2008). Such information on oblique impact directionality given by impact crater/basin shape is important in terms of characterizing potential antipodal effects. Through experimental and modeling means, Schultz & Crawford (2011) demonstrated that substantial disruption of the lunar surface antipodal to the initial contact site of the South Pole-Aitken (SPA) Basin-creating impactor would have taken place. They also noted that the center of the resulting topographic basin was offset downrange from the location of first contact. Based on these findings, they proposed an oblique impact scenario that produced a system of radial and circumferential tectonics covering much of the lunar near side, roughly

antipodal to SPA. The antipodal effects demonstrated by their experimental and modeling work are worth considering for Pluto.

In Figure 10 we identify four locations within SP that are related to the impact process. The pink star in Figure 10 represents the potential first-contact point of an oblique impactor approaching from the NNW. The red triangle marks the approximate center of the deep basin portion of SP (i.e., where the nitrogen ice is thick enough to support convection, McKinnon et al. 2016), identified as "the basin center." The yellow circle marks the transition from the basin center to the southern portion of SP, where the onset of non-cellular plains suggests that the nitrogen ice is not convecting here and is shallower than in the basin center (McKinnon et al. 2016; White et al. 2017). The blue diamond marks a potential first-contact point of an oblique impactor approaching from the SSE. Figure 11 shows the corresponding antipode locations of each of these on the FS. Under a scenario where the approach of the SP-forming impactor was from the NNW, the antipode of the initial site of impact falls beyond the southern limit of the imaged portion of the far side, in the dark southern latitudes (see the pink star in Figure 11).

If the incidence direction of the SP forming impact were from the SSE, then the excavated region widened until an ultimate circular-margined basin was produced. Under this scenario, the elongation could reflect fracture and ricochet of impactor fragments terminating in a circular crater downrange, as found in laboratory experiments and observed in planetary settings (Schultz & Gault 1990). Alternatively, an approach from the NNW requires downrange narrowing of the crater with no terminal round crater at extremely low incidence angles (Schultz & Gault 1990; Elbeshausen et al. 2013), resembling observed downrange narrowing at Martian craters such as Orcus Patera. The SSE incidence scenario may potentially account for the complex appearance of surface features located in a >1000 km diameter zone surrounding the first contact antipode (blue diamond in Figure 11), which includes the large-scale lineations of unit *dd* as well as the occurrences of the bladed terrain deposits (unit *btd*) and mottled, dark terrain (unit *mdt*) with especially angular and irregular planforms between 340°E and 10°E. The rather chaotic and intricate configuration of terrains within this zone may reflect disruption of Pluto's crust and surface topography in response to the Sputnik basin-forming impact, perhaps similar to the

chaotic terrain seen antipodal to the Caloris basin on Mercury (Schultz & Gault 1975). Such disruptions may include contributions from antipodal tectonics and deposition of ejecta at the antipode (Wieczorek & Zuber 2001).

In the analysis just presented, we considered the possibility that effects of the RTS and/or the SP basin-forming impact are manifested within the geology of the far side between 330°E and 30°E. However, the quality of the FS data is insufficient to distinguish which elements of the geology may be due to one phenomenon or the other, or to determine if there are other geological processes besides these that are also affecting its appearance. Further analysis of this region would benefit tremendously from improved resolution in the future.

5. Additional Considerations Regarding Simonelli Crater And the Far Side Maculae

Here we discuss two other specific and notable implications of the far side datasets and maps.

Simonelli Crater. The largest identifiable impact crater on the mapped FS is Simonelli, which at 250 km diameter rivals the largest identified impact crater on the near side hemisphere, Burney (~290 km diameter). Simonelli is located at the same latitude (12°N) as Elliot crater on the near side hemisphere, which places both at the northern limit of the permanent diurnal zone (13°N), and which also marks the northern limit of the dark surface layer that defines Cthulhu and other maculae. Both Simonelli and Elliot have central peaks and high albedo floors, suggesting a common physical process of axially symmetric volatile deposition around the central peak. The NS craters Oort and Edgeworth are also of broadly comparable size, but are located slightly farther south (~7.5° N) within Cthulhu Macula, and do not show high albedo floors. Whether this is related to their presence within Cthulhu Macula, or is due to some other cause, is unclear, but nonetheless demonstrate that high albedo crater floors as seen in Elliot and Simonelli are not universal on Pluto for craters of this size or even this latitude zone.

The Far Side Maculae and Their Relation to Bladed Terrain Deposits. Far side mapping has revealed that the maculae there (which refer to the maculae stretching from Krun to Meng-p'o Maculae, mapped as unit *mtd*, in Figure 5) are smaller in scale and more fragmented than the sprawling Cthulhu Macula of the NS. Krun Macula and a small portion of Ala Macula are the only near side representative of these smaller-scale maculae. Krun's geology appears markedly more evolved than that of Cthulhu Macula, displaying rugged, collapsed, lightly cratered terrain. This is in contrast to the flat, and more extensively cratered plains of Cthulhu Macula, which appear relatively unmodified since the heavy bombardment era and are interpreted to have accumulated a layer of haze or irradation-derived dark, red particles over the last 4.5 Gyr (Grundy et al., 2018). The non-collapsed, and therefore relatively pristine, portions of Krun Macula typically reach 1.5 to 2.5 km (and even as much as 4 km) in elevation, comparable to the lower portions of the bladed terrain deposits of Tartarus Dorsa, which Krun Macula borders at its eastern end. The plains of western Cthulhu Macula, by comparison, range from 0 to 2 km in elevation. Krun Macula therefore represents an evolved landscape that is blanketed by haze or irradiation-derived particles and yet also rises to elevations where bladed terrain deposits would normally be expected to occur within this upland region of the permanent diurnal zone east of Sputnik Planitia. In addition, the sinuous contact between Krun, Ala Maculae, and Tartarus Dorsa appears gradational, with the bladed texture becoming darker and less distinct with increasing proximity to the maculae ('2' labels in Figure 6a).

It appears from the available data that the close spatial relationship between maculae and bladed terrain deposits continues into the far side. The contact between units *mdt* and *btd* is intricate and angular, and both units embay occurrences of the other (see Figure 5). The elevation of the far side maculae is more difficult to confidently determine: like Krun Macula, the portions of Hun-Came and Meng-p'o Maculae that are crossed by profile C in Appendix A, Figure A1, do appear to be elevated relative to Cthulhu Macula, but it cannot be discounted that this may be due to protruding off-limb topography of the bladed terrain deposits obscuring the true relief of the maculae. Yet Krun Macula proves that maculae can rise to elevations comparable to the bladed terrain deposits, raising the question of how maculae with a relatively young crater age would originate within high elevation

regions of the diurnal zone of the western far side that would otherwise be natural locations for deposition of methane to form the bladed terrain deposits.

We now hypothesize two scenarios for how the geologic history of the FS maculae and bladed terrain deposits may be intertwined (see Figures 12A and 12B), each of which involves recession of the bladed terrain deposits by sublimation in response to secular climate change (Moore et al., 2018). The first scenario is that the evolved climatic conditions and morphology of the bladed terrain deposits resulted in conditions favoring mobilization of surface methane ice being suppressed for large expanses of relatively low elevation bladed terrain deposits compared to those at higher elevation. Such mobilization was then interrupted for long enough (millions of years) to allow a layer of haze or irradiation-derived particles to accumulate on these "deactivated" bladed terrain deposits (Grundy et al. 2018) and reach a sufficient thickness to inhibit further large scale volatile mobilization (see Figure 12A). Alternatively, the maculae may represent regions where the deposits have been stripped away by the recession, as is hypothesized to have occurred at the northern margin of Tartarus Dorsa (Moore et al., 2018), thereby exposing the elevated water ice crust onto which they were emplaced (see Figure 12B). In this scenario, the low albedo of the exhumed terrain represents the original blanket of haze or irradiation-derived particles that this crust, located within the permanent diurnal zone, accumulated prior to emplacement of the bladed terrain deposits (Bertrand & Forget 2019), and which is currently re-accreting haze or irradiation-derived particles now that it is once again exposed to the atmosphere.

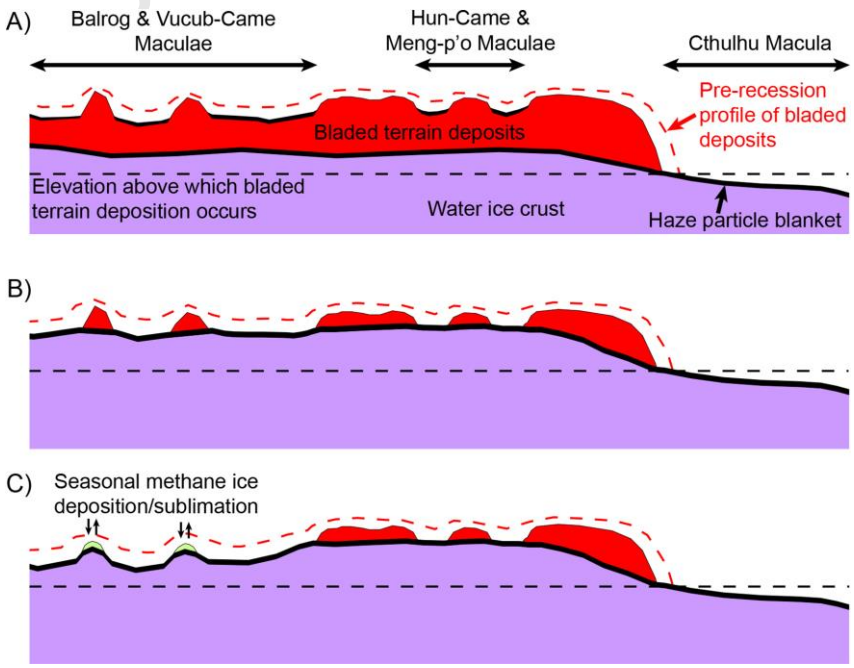

Figure 12. Origin/evolution scenarios hypothesized for the far side maculae. Cross sections extend from Balrog Macula in the west to the low elevation plains of western Cthulhu Macula in the east, at a latitude of ~10°S. The vertical dimension is exaggerated. (A) Low elevation portions of bladed terrain deposits accumulate a blanket of haze particles. (B) Portions of the bladed terrain deposits are entirely stripped away, revealing the dark haze blanket covering the water ice crust underneath. (C) The wispy terrain seen within Balrog and Vucub-Came Maculae does not represent bladed terrain deposits, but rather thin, seasonal deposits of methane ice superposed on the haze blanket in elevated and topographically prominent locations.

The first of these two scenarios interprets the wispy texture that characterizes the mottled, dark terrain of Balrog and Vucub-Came Maculae in imaging of several km/pixel to be outcrops of bladed terrain deposits that are rising above the surrounding maculae. Yet the scale of the wispy texture is at the limit of image resolution here. So the second scenario interprets the wispy texture as thin seasonal accumulations of CH_4 ice on a scale of several km to tens of km across that have deposited onto the maculae (see Figure 12C). On the near side, such methane deposits are seen at the summits of Pigafetta Montes in eastern Cthulhu Macula, which may be perennially stable, and on north-facing walls of craters in their vicinity, which are likely seasonal (Bertrand & Forget 2019). Volatile transport modeling by Bertrand & Forget (2019) indicates that despite the low albedo of the macula, which has the effect of raising the daytime surface temperature, nighttime conditions in the diurnal zone are still sufficiently cold to permit deposition of CH_4 ice where high surface winds and sufficiently high atmospheric CH_4 content allow. Once established as a thin surface layer, further CH_4 deposition can be supported due to the higher albedo of the ice, although the Pigafetta and crater deposits are too small for runaway albedo feedback to be sustained that would allow for the accumulation of sprawling bladed terrain deposits. If small-scale, ephemeral CH_4 ice deposits like these are represented within the wispy portions of unit *mdt*, then their configuration would change with the seasons as the CH_4 ice sublimates

away to higher latitudes, revealing the dark substrate, and later returns to the maculae to reform on slopes of different aspect.

6. Geological History

Figure 13 follows Skinner et al. (2018) to present a correlation of most of the map units in Figure 5, and serves to represent how mapped geological units are oriented in space and time relative to one another and established geologic time scales, where known.

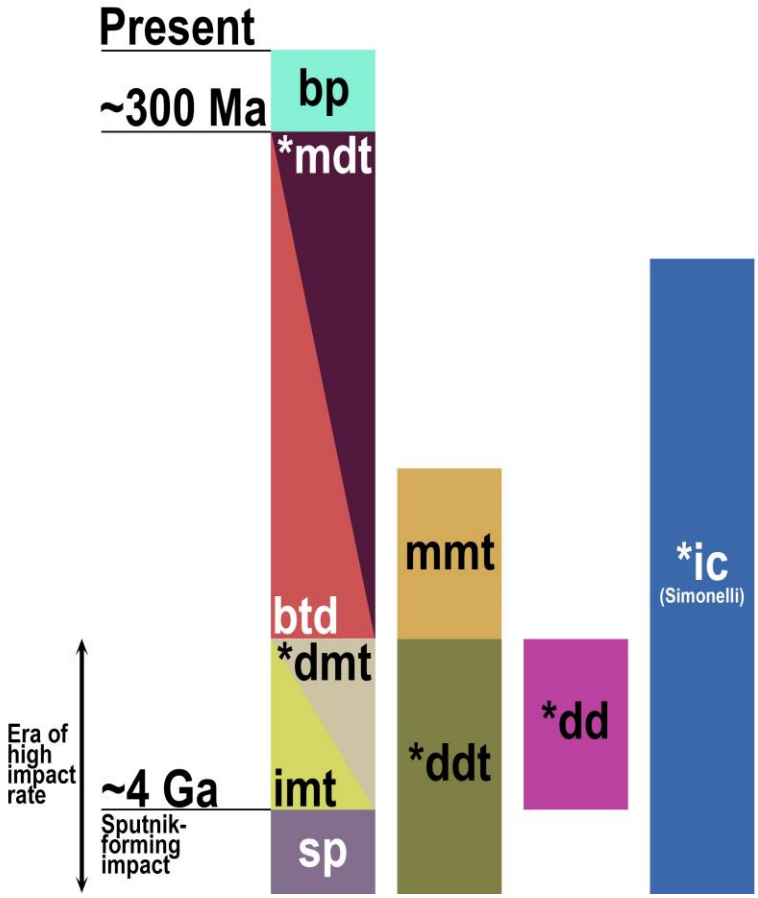

Figure 13. Correlation chart of FS geologic units mapped in Figure 5, excepting *um* and *ltm*, the natures of which are undetermined. Time runs from bottom to top here over Pluto's history. Stratigraphic positions have been determined by crosscutting and superposition relations where available and topographic relief of the units where revealed in limb profiles, as well as crater size-frequency distributions of the units where expressed in the near side hemisphere, although

asterisked units indicate those for which age relationships are based mainly on process interpretations (e.g. one unit transforming into another) rather than stratigraphy/crater observations. Unit boxes that are contiguous (*btd*/*mdt* and *imt*/*dmt*) are to indicate a close formative association. The top and bottom of each unit box corresponds to our assessment of the time scale of the formation and subsequent modification, if any, of each unit.

The earliest apparent FS unit is the smooth plains (unit *sp*) of western Cthulhu Macula, which display a high crater count (e.g., Singer et al. 2019), and may have formed approximately contemporaneously with the Sputnik basin-forming impact ≳4 Ga, or may possibly predate that. Consisting of inert H_2O-ice crust located within the permanent diurnal zone (Binzel et al. 2017), this terrain has apparently experienced minimal modification by exogenic processes since it formed, save for (i) accumulating a thin layer of ice irradiation- or atmospheric sedimentation-derived haze particles (Grundy et al. 2018) and (ii) overprinted volatile transport, most evident in Cthulhu Macula's eastern regions, particularly at Pigafetta Montes.

The immediate post-Sputnik impact era (~4 Ga) likely witnessed the original emplacement of the bright, methane-rich mantle that covers Venera and Vega Terrae in the northwest of the NS hemisphere. The higher latitudes within the FS were also then mantled, forming the intermediate, mantled terrain (unit *imt*), which underwent extensive sublimation erosion in the mid-latitudes to form the dark, mantled terrain (unit *dmt*). This era was apparently characterized by a high impact rate, and these mantled terrains, like the smooth plains, exhibit high crater counts where they are seen on the near side (Singer et al. 2019).

Separate occurrences of the dark depressions (unit *dd*) may have different formation mechanisms, but we speculated above that the regional-scale lineations formed by this unit between 330°E and 0°E may represent an extension of a giant north-south-aligned tectonic system that bisects the near side hemisphere (Schenk et al. 2018), or alternatively may indicate crustal disruption antipodal to the Sputnik basin-forming impact. Both hypotheses place the formation of these lineations at ~4 Ga, and if their floors are exposing water ice crust, then

they must cut through (and therefore postdate) the surrounding intermediate, mantled terrain. Besides the fact that the bladed terrain deposits (unit *btd*) crosscut unit *dd*, there is no other observational way to confirm its relative age position, as crater counts are not possible at the available mapping resolution. The uniquely shaped dark crescent of Yutu Linea may instead indicate an ancient impact crater or basin that was superposed by the mantling material of unit *imt*, with the mantle subsequently eroding away at the southern and eastern walls of the crater, as appears to have happened for Guest crater on the near side. Alternatively, Yutu Linea could be a signature of tectonics antipodal to Sputnik.

A thicker mantling deposit postdating that in Venera and Vega Terrae, then apparently covered Pioneer and Hayabusa Terrae to the northeast of Sputnik Planitia. This mantling, which displays fewer impact craters compared to Venera and Vega Terrae (Singer et al. 2019), was likely emplaced as the impact rate was waning (i.e., <4 Ga), and may have been in part or whole sourced via gaseous emissions from large, deep pits in Pioneer Terra (Howard et al. 2017). The mottled, mantled terrain (unit *mmt*) within the FS appears to represent its eastern extent, and appears to be partly eroded via sublimation.

The equatorial bladed terrain deposits (unit *btd*) likely originated during an episode of massive precipitation of atmospheric CH_4 at high elevation within Pluto's low latitude diurnal zone, where time-averaged insolation is at a minimum (Binzel et al. 2017; Moore et al. 2018). The *btd* crosscut and so postdate the majority of units that they contact, including the smooth equatorial plains of Cthulhu Macula and the dark depressions and intermediate mantled terrain of the higher latitudes. Volatile transport modeling has shown that deposits reaching a kilometer thick can form in the space of 50-100 Myr (Bertrand et al. 2019), and also that it is plausible for perennially stable CH_4 ice deposits to form on the maculae (Bertrand & Forget 2019), meaning that the original emplacement of the bladed terrain deposits need not necessarily have occurred in Pluto's ancient history, prior to the darkening of the equatorial zone.

Subsequent secular excursions in Pluto's climate seem to have partially eroded the bladed terrains via sublimation, and may also have erased

some impact craters. Where they occur within the near side hemisphere (e.g., Tartarus Dorsa), the bladed terrains are virtually un-cratered (Singer et al. 2019) and exhibit a likely surface age of just ~200 to 300 Ma (Moore et al. 2018). On the FS, it is not certain whether Simonelli crater (unit *ic*) impacted into these deposits, or if these deposits colonized the pre-existing Simonelli. Recession of the deposits exhumed terrain that they previously superposed, including the dark, degraded terrain at their northern margin (unit *ddt*). The exact nature of the far side maculae, mapped as the mottled, dark terrain (unit *mdt*) is uncertain, but their relatively high topographic relief (most obvious for the well resolved, near side Krun Macula) and close geographical association with the bladed terrain deposits implies that the two units could be genetically related. The mottled, dark terrain may represent relatively low elevation deposits where mobilization of the surface CH_4 ice became inactive as the configuration of the deposits changed as they receded, or alternatively a H_2O ice substrate that was exhumed after the bladed terrain deposits were completely stripped away by such recession. Both scenarios would result in the presentation of a dark layer of particles at the surface, either through the accumulation of a fresh layer of particles, or the exhumation of an old dark surface that underlies the deposits. Some seasonal CH_4 ice deposition also may be occurring in Balrog and Vucub-Came Maculae, as is seen in eastern Cthulhu Macula.

The bright plains (unit *bp*) superpose units *btd* and *mdt*, and are unequivocally the youngest terrain on the FS, interpreted to represent craterless, predominantly nitrogen ice that has condensed on the floors of depressions amongst the bladed terrain deposits, as seen in East Tombaugh Regio and Tartarus Dorsa in the near side hemisphere (Moore et al. 2018), and which is presently undergoing sublimation and glacial flow. The undifferentiated material (unit *um*) and the light-toned material (unit *ltm*) are the least interpretable units on the FS, and accordingly the timing of their formation cannot yet be determined.

7. Summation and Next Steps

New Horizons data demonstrates that Pluto's far side hemisphere displays a notably different terrain mix than the planet's near side

hemisphere. Among the prominent expressions seen on the FS are: (i) evidence for the extensive global bladed terrain deposits not seen on the near side hemisphere; (ii) maculae that have different character than Cthulhu (dominating the NS hemisphere's maculae); and (iii) an enigmatic complex of lineations that is crudely antipodal to and may relate to the origin of the SP forming event.

Future progress on far side geology, geophysics, and compositional studies would benefit tremendously from a Pluto orbiter. In particular, such an orbiter could address the key far side related questions including:

- What is the global distribution of Pluto's volatile units, and how does this relate to Pluto's climatic history?

- What is the nature of Pluto's great ridge-trough system (RTS), and is it truly global?

- How did Sputnik Planitia form, and did its formation play a significant role in shaping the FS geology of Pluto?

- What is the nature of the FS maculae, i.e., is their origin really tied to the bladed terrain deposits, and to what extent are they currently host to sublimating seasonal volatiles?

Since the arrival of any such orbiter is unfortunately at least two decades away, in the nearer term we must rely on advances that can be obtained from observatories with new capabilities on or near Earth, and on laboratory and modeling efforts.

Most notable among the possibilities for relevant new observations from Earth or Earth orbit will be the new generation of 25-to-30 m diameter telescopes coming on line in the 2020s. These devices will have diffraction limited resolutions ~10x better than Hubble Space Telescope, and will be able to obtain panchromatic, color, and even compositional spectroscopic maps of Pluto with resolutions of 30-50 km on a regular basis. The resolution of such maps will not surpass the New Horizons FS mapping discussed in this paper, but will allow many more colors to be explored, and will also permit studies of surface time

variability as Pluto's seasons advance over the coming decades. In addition to yielding new knowledge about Pluto itself, the comparison of these dataset to similar datasets obtained on Triton and other Kuiper Belt dwarf planets will also inform our understanding of the range of surface variation and variegation on such planets as a class. Time-dependent James Webb Space Telescope (JWST) and Atacama Large Millimeter Array (ALMA) will also be important, enabling thermal mapping at crudely similar resolution in the coming decades.

Acknowledgements

This work was supported, except as otherwise noted, by NASA's New Horizons mission. PJM was supported by NASA's New Frontiers Data Analysis Program grant 80NSSC18K1317, from which OLW also received partial support. We acknowledge helpful comments from our colleague Tanguy Bertrand, referee Geoff Collins, and another (anonymous) referee. This paper is dedicated to the future spacecraft exploration of Pluto's fascinating far side.

Appendix A
Topographic Data Types

Stereogrammetry, Photoclinometry, and Terminators. Stereogrammetric mapping of FS topography was obtained in areas north of ~50° latitude (Schenk et al. 2018). However, all attempts to derive coherent stereogrammetric Digital Elevation Model (DEM) data product southward of this in the FS were unsuccessful due to a combination of low parallax, low resolution, and low (likely <6 km; Schenk et al. 2018) inherent relief of these areas. We further note that photoclinometry cannot be reliably used in the low-resolution part of the FS mapping coverage due to severe albedo contrasts and the lack of significant resolvable shadowing.

However, topography can manifest itself as deviations along the terminators in approach images, although the quantitative limit on the scale of topographic variations that can be detected differs with changing image resolution across the far side during the New Horizons approach to Pluto. As shown in Figure 1, at its western boundary, FS terminator imaging achieves a pixel scale of ~2 km/pixel, while at its eastern boundary, such imaging is limited to >30 km/pixel. Features with the highest local topographic relief on the near side reach >6 km above their immediate surroundings (i.e., the taller mountains above Sputnik Planitia; see Schenk et al. 2018). Assuming that local topographic relief on the FS does not exceed this value, it follows that imaging achieving a pixel scale of 6 to 7 km/pixel is the likely limit for which any local topographic relief that would realistically be detectable there (i.e., appearing as pixel-wide deviations).

Figure 1 shows that the region covered by imaging at this pixel scale or better extends as far east as ~275°E at the equator (i.e. to the western portion of Balrog Macula). Deviations in the terminator seen in imaging to the west of this are interpreted to be bladed terrain deposits with topographic relief of 2-3 km. Simonelli crater, located at 12°N, 315°E, is covered in terminator imaging of ~11 km/pixel; while its topographic relief is not sufficient to be detectable as a deviation in the terminator, its shading at high phase does confirm that it is a central peak crater (see Figure 8). While the coarse pixel scale of imaging in the eastern portion of the NS hemisphere precludes our ability to identify

topographic features with relief of <10 km in terminator imaging there, it is sufficient to conclude that no extremely high "Olympus Mons" or deep "Valles Marineris" type features with relief exceeding 10 km are revealed in the sunlit terrains there.

Limb Profiles. The lack of high-resolution images of Pluto's FS and the lack of stereo topography except in the FS north require the use of alternative methods to derive topographic information. Topographic profiles for these regions can still be obtained by careful measurements of the limb in both close encounter and post-encounter backlit FS images. These two types of image illumination require slightly different techniques for accurately determining limb positions. For standard images (i.e., on the day side of Pluto) we use Method A of Nimmo et al. (2017). This scans each row and column in the image away from the body center. In each scan the limb is taken to be the point where the brightness is half way between the face and background value; see Nimmo et al. (2017) for details.

In backlit images, the disk of Pluto and the background are dark to within the noise of the camera. There is, however, some forward scattered light from atmospheric hazes, which is brightest near Pluto and fades farther from the disk. The sharp contrast between the dark disk and the bright haze is captured very clearly by taking the gradient of the image. Therefore, in backlit images (MVIC scan 0299181722), each row and column of the image was scanned away from the body center, and the limb was taken to be the location of the maximum in image gradient magnitude. For the backlit MVIC scan 0299181303, low signal to noise ratios prevented this gradient approach from working consistently. For this image, when scanning each row and column the limb was taken to be the point when the pixel brightness exceeded a set threshold. For all methods, spurious limb picks caused by cosmic ray hits or other artifacts were manually removed.

We have however used limb profiles extracted from four New Horizons observations in our geological mapping and analysis, shown alongside their ground tracks in Figure A1. These include two LORRI observations (one front lit and one back lit) and two MVIC observations (both back lit), both located within the eastern half of the FS. These each have a pixel scale of <1 km/pixel, sufficient to resolve FS topographic relief.

These images each have a pixel scale of <1 km/pixel, which is sufficient to resolve FS topographic relief. For the MVIC profiles, we apply a high-pass filter at 1000 km to remove the long-wavelength signal associated with spacecraft motion during scanning. This renders short wavelength topography accurate to within 5% error These profiles are annotated with the locations of units mapped in Figure 5, and supplement the profile shown in Schenk et al. (2018).

We note however that important considerations must be taken into account when interpreting topography expressed in these limb profiles. Landforms within the profiles that show positive topographic relief (e.g. hills and mountains) may not necessarily be located directly on the limb ground track, but could be instead located within the foreground or background with respect to the limb, with the crest of the landform protruding above the limb. Only if such a landform is located on the limb itself will the topography in the limb profile be representative of its total topographic relief. Landforms with positive topographic relief therefore tend to be more apparent within limb profiles compared to landforms with negative topographic relief (e.g., pits and craters), as off-limb landforms with positive topography often obscure the negative topographic signature of depressions located on the limb. The apparent relief of a depression as seen in a limb profile will rarely be representative of its total depth, and only if both the foreground and background topography are also depressed. Pluto's atmosphere and its haze layers provide an unusual opportunity in the case of profile B. This limb profile was extracted from an observation where the haze on the FS is brightly backlit by the Sun, to the extent that the haze dimly illuminates some foreground topography. This reveals additional clues about what on-limb and off-limb landforms are responsible for the topography seen in the limb profile, an attribute that is not shared by the more dimly backlit C and D limb profiles. Profile B is examined in the discussion of the dark depressions unit in Section 3.

Careful comparison between the limb profiles and the base map is therefore warranted, in order to assess what features in the limb profile may be caused by off-limb topography. Where possible, examination of multiple profiles that cross a particular unit help in determining that unit's characteristic topographic signature with respect to other units that border it. These considerations are particularly relevant to

determining the topographic relief of the FS maculae, and to distinguishing between high elevation terrains there that are indicative of bladed terrain deposits versus those that are indicative of other landforms.

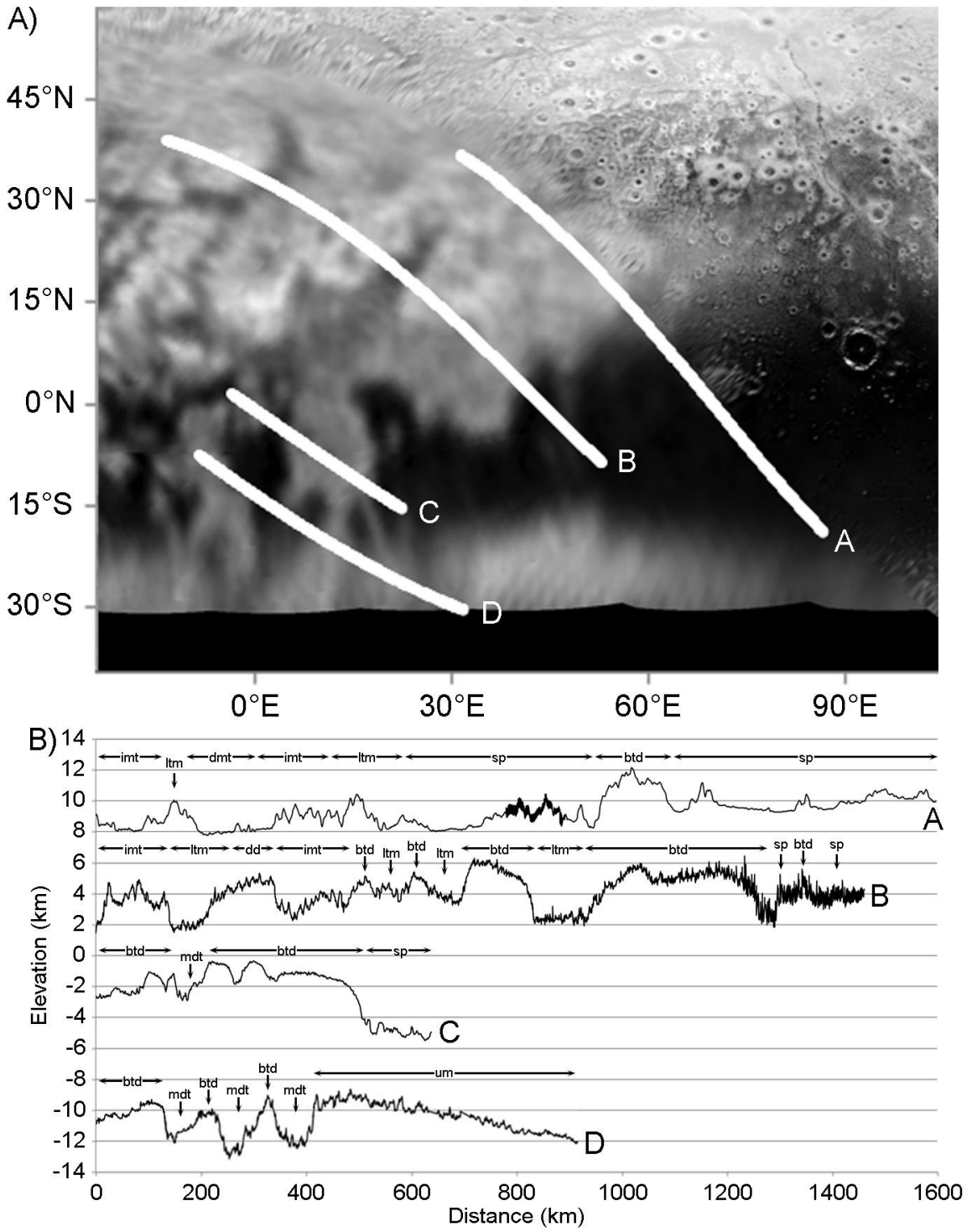

Figure A1. Panel A: Ground tracks of the four limb profiles shown in Panel B. Profile A was extracted from a mosaic of three 889 m/pixel LORRI frames (0299168423, 0299168039, and 0299167992). Profile B was extracted from a mosaic of three 805m/pixel LORRI frames (0299192233, 0299192286, and 0299192339). Profile C was extracted from a 346 m/pixel MVIC scan (0299181303). Profile D was extracted from a 431 m/pixel MVIC scan (0299181722). Panel B: Profiles A-D, annotated with the locations of mapped units in Figure 5. Note that unit *dd* in profile B appears high because the depressed topographic signature of the lineation that the profile crosses here is being masked by background topography (see Figure 7).

References

Andrews-Hanna, J. C., M. T. Zuber, W. B. Banerdt (2008). The Borealis basin and the origin of the Martian crustal dichotomy. *Nature* **453**, 1212-1215. doi: 10.1038/nature07011

Bertrand, T., and Forget, F. (2016). Observed glacier and volatile distribution on Pluto from atmosphere-topography processes. *Nature* **540**, 86-89, doi:10.1038/nature19337

Bertrand T. and Forget F. (2019). How seasonal methane snow forms on Pluto on mountaintops, crater rims, and slopes. *American Geophysical Union Fall Meeting 2019*, San Francisco, CA, Abstract #P42C-06.

Bertrand, T., Forget, F., Umurhan, O.M., et al. (2019). The CH_4 cycles on Pluto over seasonal and astronomical timescales. *Icarus* **329**, 148-165, doi: 10.1016/j.icarus.2019.02.007

Bertrand, T., Forget, F., White, O., Schmitt, B., Stern, S. A., Weaver, H., Young, L. A., Ennico, K., Olkin and C. B. Olkin (2020). Pluto's beating heart regulates the atmospheric circulation: Results from high-resolution and multiyear numerical climate simulations. Journal of Geophysical Research: Planets, 125, e2019JE006120.

Binzel R. P., Earle A. M., Buie M. W., et al. (2017). Climate zones on Pluto and Charon. *Icarus* **287**, 30-36. doi: 10.1016/j.icarus.2016.07.023

Buie, M. W., Tholen, D. J, Horne, K. (1992). Albedo maps of Pluto and Charon: Initial mutual event results. *Icarus* **97**, 211-227. doi: 10.1016/0019-1035(92)90129-U

Buie, M. W., Young, E. F., Binzel, R. P. (1997). "Surface Appearance of Pluto and Charon," in *Pluto and Charon* (S. A. Stern, D. J. Tholen, eds.), University of Arizona Press, Tucson, pp. 269-293.

Buie, M. W., Grundy, W. M., Young, E. F., Young, L. A., Stern, S. A. (2010). Pluto and Charon with the Hubble Space Telescope. II. Resolving Changes on Pluto's Surface and a Map for Charon. *AJ* **139**, 1128-1143. doi: 10.1088/0004-6256/139/3/1128/meta

Buratti, B. J., Hofgartner, J. D., Hicks, M. D., et al. (2017). Global albedos of Pluto and Charon from LORRI New Horizons Observations. *Icarus* **287**, 207-217. doi: 10.1016/j.icarus.2016.11.012

Cheng, A. F., Weaver, H. A., Conard, S. J., et al. (2008). Long Range Reconnaissance Imager on New Horizons. *Space Sci. Rev*. **140**, 189-215. doi: 10.1007/s11214-007-9271-6

Earle, A. M., Binzel, R. P., Young, L. A., et al. (2017). Long-term surface temperature modeling of Pluto. *Icarus* **287**, 37-46. doi: 10.1016/j.icarus.2016.09.036

Earle, A. M., Binzel, R. P., Young, L. A., et al. (2018a). Albedo matters: Understanding runaway albedo variations on Pluto. *Icarus* **303**, 1-9. doi: 10.1016/j.icarus.2017.12.015

Earle, A. M., Grundy, W., Howett, C. J. A., et al. (2018b). Methane distribution on Pluto as mapped by the New Horizons Ralph/MVIC instrument. *Icarus* **314**, 195-209. doi: 10.1016/j.icarus.2018.06.005

Elbeshausen, D., Wünnemann, K., Collins, G. S. (2013). The transition from circular to elliptical impact craters. *J. Geophys. Res.* **118**, 2295-2309. doi: 10.1002/2013JE004477

Gabasova, L.R., et al. (2020). Global compositional cartography of Pluto from intensity-based registration of LEISA data. *Icarus*, submitted.

Garrick-Bethell, I., and Zuber, M. T. (2009). Elliptical Structure of the Lunar South Pole-Aitken Basin. *Icarus* **204**, 399. doi: 10.1016/j.icarus.2009.05.032

Gladstone, G. R., Stern, S. A., Ennico, K., et al. (2016). The atmosphere of Pluto as observed by New Horizons. *Science* **351**, aad8866. doi: 10.1126/science.aad8866

Grundy W. M., Binzel R. P., Buratti B. J., et al. (2016). Surface compositions across Pluto and Charon. *Science* **351**, aad9189. doi: 10.1126/science.aad9189

Grundy W. M., Bertrand T., Binzel R. P., et al. (2018). Pluto's haze as a surface material. *Icarus* **314**, 232-245. doi: 10 .1016/j.icarus.2018.05.019

Hammond, N. P., and Barr, A. C. (2014). Global resurfacing of Uranus's moon Miranda by convection, *Geology* **42**, 931–934. doi: 10.1130/G36124.1

Howard, A. D., and M. J. Selby (2009). "Rock slopes," in *Geomorphology of Desert Environments* (A. J. Parsons, A. D. Abrahams, eds.), Springer, pp. 189-232.

Howard, A. D., Moore, J. M., White, O. L., et al. (2017). Pluto: Pits and mantles on uplands north and east of Sputnik Planitia. *Icarus* **293**, 218-230. doi: 10.1016/j.icarus.2017.02.027

Johnson, B. C., Bowling, T. J., Trowbridge, A. J., Freed A. M. (2016). Formation of the Sputnik Planum basin and the thickness of Pluto's subsurface ocean. *Geophys. Res. Lett.* **43**, 10,068-10,077. doi: 10.1002/2016GL070694

Kamata, S., et al. (2019). Pluto's ocean is capped and insulated by gas hydrates. *Nature Geoscience*, **12**, 407–410.

Keane, J. T., Matsuyama, I., Kamata, S., Steckloff, J. K. (2016). Reorientation and faulting of Pluto due to volatile loading within Sputnik Planitia. *Nature* **540**, 90-93. doi: 10.1038/nature20120

Matsuyama, I., Nimmo, F., Mitrovica, J. X. (2014). Planetary reorientation. *Annu. Rev. Earth Planet. Sci.* **42**, 605–634. doi: 10.1146/annurev-earth-060313-054724

McGovern, P. J., White, O. L., Schenk, P. M. (2019). Tectonism across Pluto: Mapping and Interpretations. *Pluto System After New Horizons*, Laurel, MD, Abstract #7063.

McKinnon, W. B., Nimmo, F., Wong, T., et al. (2016). Convection in a volatile nitrogen-ice-rich layer drives Pluto's geological vigour. *Nature* **534**, 82-85. doi: 10.1038/nature18289

Melosh, H. J. (1980). Tectonic patterns on a reoriented planet: Mars. *Icarus* **44**, 745-751. doi: 10.1016/0019-1035(80)90141-4

Moore, J. M., McKinnon, W. B., Spencer, J. R., et al. (2016). The geology of Pluto and Charon through the eyes of New Horizons. *Science* **351**, 1284-1293.doi: 10.1126/science.aad7055

Moore, J. M., Howard, A. D., Umurhan, O. M., et al. (2018). Bladed Terrain on Pluto: Possible origins and evolution. *Icarus* **300**, 129-144. doi: 10.1016/j.icarus.2017.08.031

Moores, J. E., Smith, C. L., Toigo, A. D., Guzewich S. D. (2017). Penitentes as the origin of the bladed terrain of Tartarus Dorsa on Pluto. *Nature* **541**, 188-190. doi: 10.1038/nature20779

Nimmo, F., Hamilton, D. P., McKinnon, W. B., et al. (2016). Reorientation of Sputnik Planitia implies a subsurface ocean on Pluto. *Nature* **540**, 94-96. doi: 10.1038/nature20148

Nimmo, F., Umurhan, O., Lisse, C. M., et al. (2017). Mean radius and shape of Pluto and Charon from New Horizons images. *Icarus* **287**, 12-29. doi: 10.1016/j.icarus.2016.06.027

Olkin, C.B., et al. (2017). The Global Color of Pluto from New Horizons, The Astronomical Journal, 154, 258-271.

Protopapa, S., Grundy, W. M., Reuter, D. C., et al. (2017). Pluto's global surface composition through pixel-by-pixel Hapke modeling of New Horizons Ralph/LEISA data. *Icarus* **287**, 218-228. doi: 10.1016/j.icarus.2016.11.028

Reuter, D. C., Stern, S. A., Scherrer, J., et al. (2008). Ralph: A visible/infrared imager for the New Horizons Pluto-Kuiper Belt mission. *Space Sci. Rev*. **140**, 129-154. doi: 10.1007/s11214-008-9375-7

Schenk, P. M., Beyer, R. A., McKinnon, W. B., et al. (2018). Basins, fractures and volcanoes: Global cartography and topography of Pluto

from New Horizons. *Icarus* **314**, 400-433. doi: 10.1016/j.icarus.2018.06.008

Schmitt, B., Philippe, S., Grundy, W. M., et al. (2017). Physical state and distribution of materials at the surface of Pluto from New Horizons LEISA imaging spectrometer. *Icarus* **287**, 229-260. doi: 10.1016/j.icarus.2016.12.025

Schultz, P. H., and Gault, D. E. (1975). Seismic effects from major basin formations on the moon and mercury, *The Moon* **12**, 159-177. doi: 10.1007/BF00577875

Schultz, P. H., and D. E. Gault (1990). "Prolonged global catastrophes from oblique impacts," in *Global Catastrophes in Earth History: an Interdisciplinary Conference on Impacts, Volcanism, and Mass Mortality* (V. L. Sharpton, P. D. Ward, eds.), Boulder, Colorado. *Geol. Soc. Am. Spec. Pap.* 247, p. 239. doi: 10.1130/SPE247-p239

Schultz, P. H. and Crawford, D. A. (2011). "Origin of nearside structural and geochemical anomalies on the Moon," in *Recent Advances and Current Research Issues in Lunar Stratigraphy* (W. A. Ambrose, D. A. Williams, eds.), *Geol. Soc. Am. Spec. Pap.* 477, pp. 141-159. doi: 10.1130/2011.2477(07)

Singer K. N., McKinnon W. B., Gladman B., et al. (2019). Impact craters on Pluto and Charon indicate a deficit of small Kuiper belt objects. *Science* **363**, 955-959. doi: 10.1126/science.aap8628

Skinner, J. A., Huff, A. E., Fortezzo, et al. (2018). Planetary Geologic Mapping Protocol-2018. USGS, Flagstaff, AZ. https://astropedia.astrogeology.usgs.gov/alfresco/d/d/workspace/SpacesStore/01e32dcd-3072-4ac2-8e41 7cc5029bd2cf/PGM_Protocol_March2018.pdf

Stern, S. A., Bagenal, F., Ennico, K., et al. (2015). The Pluto system: Initial results from its exploration by *New Horizons*. *Science* **350**, aad1815. doi: 10.1126/science.aad1815

Stern, S. A., Kammer, J. A., Barth, E. L., et al. (2017) Evidence for Possible Clouds in Pluto's Present-day Atmosphere. *Astron. Journ.*, **154**:43,mdoi:10.3847/1538-3881/aa78ec

Stern S. A., Grundy, W. M., McKinnon, W. B., Weaver, H. A., Young, L. A. (2018). The Pluto system after New Horizons. *ARAA*, **56**, 357-392. doi: 10.1146/annurev-astro-081817-051935

Weaver, H.A., Buie, M.W., Buratti, B.J., et al. (2016). The small satellites of Pluto as observed by New Horizons. *Science*, 351, 1281. aae0030

White, O. L., Moore, J. M., McKinnon, W. B., et al. (2017). Geological mapping of Sputnik Planitia on Pluto. *Icarus* **287**, 261-286. doi: 10.1016/j.icarus.2017.01.011

Wieczorek, M. A., and Zuber M. T. (2001). A Serenitatis origin for the Imbrian grooves and South Pole-Aitken thorium anomaly. *J. Geophys. Res.* **106**, 27,853-27,864. doi: 10.1029/2000JE001384

Young, E. F., and Binzel, R. P. (1993) Comparative Mapping of Pluto's Sub-Charon Hemisphere: Three Least Squares Models Based on Mutual Event Lightcurves, *Icarus* **102**, 134-149. doi: 10.1006/icar.1993.1038

Young, E. F., Galdamez, K., Buie, M. W., Binzel, R. P., and Tholen, D. J. (1999). Mapping the Variegated Surface of Pluto. *AJ* **117**, 1063-1076. doi: 10.1086/300722

Young, E. F., Binzel, R. P., and Crane, K. (2001). A Two-Color Map of Pluto's Sub-Charon Hemisphere. *AJ* **121**, 552-561. doi: 10.1086/318008

Highlights

Pluto's New Horizons non-encounter (i.e., 'far side') hemisphere is explored

Maps are presented and interpreted

Important geological and geophysical conclusions are reached regarding the far side